MICROCOPY RESOLUTION TEST CHART
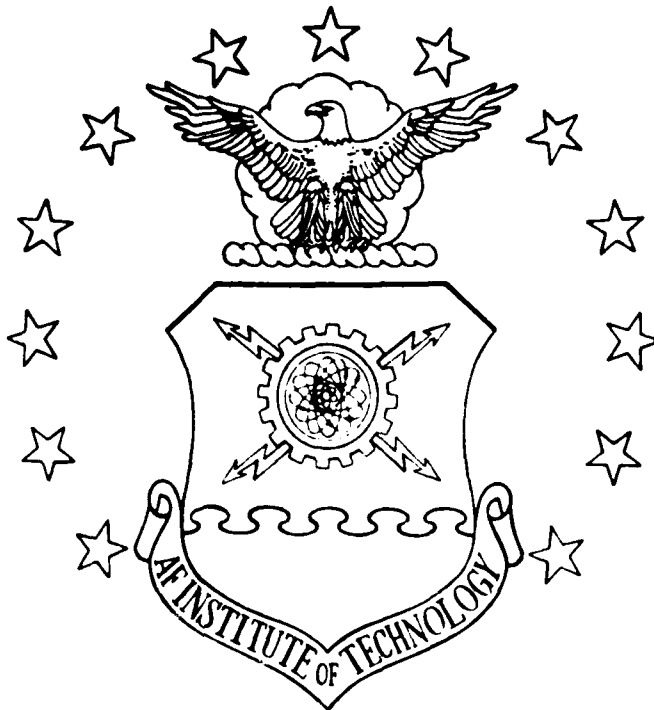
NATIONAL BUREAU OF STANDARDS - 1963 - A

AD-A135874

REANALYSIS METHODS FOR STRUCTURES

WITH LASER INDUCED DAMAGE

THESIS

AFIT/GAE/AA/83M-1   Sheryl K. Bryan
                          1st Lt   USAF

DTIC
ELECTE
DEC 1 4 1983
S
B

DTIC FILE COPY

DEPARTMENT OF THE AIR FORCE
AIR UNIVERSITY (ATC)
AIR FORCE INSTITUTE OF TECHNOLOGY

Wright-Patterson Air Force Base, Ohio

83 12 13 234

REANALYSIS METHODS FOR STRUCTURES

WITH LASER INDUCED DAMAGE

THESIS

AFIT/GAE/AA/83M-1   Sheryl K. Bryan
                          1st Lt   USAF

Approved for public release; distribution unlimited

REANALYSIS METHODS FOR STRUCTURES

WITH LASER INDUCED DAMAGE

THESIS

Presented to the Faculty of the School of Engineering

of the Air Force Institute of Technology

Air University

In Partial Fulfillment of the

Requirements for the Degree of

Master of Science

by

Sheryl K. Bryan, B.S.

1st Lt   USAF

Graduate Aerospace Engineering

March 1983

Preface

Through the years much time and effort has gone into the study of the laser, laser interactions and damage reanalysis techniques. I consider myself fortunate to have had the opportunity to merge these technologies. The result of this report is a computer program which analyzes the strength of a structure having encountered a laser strike.

I wish to acknowledge my appreciation of my thesis advisor, Dr. Peter J. Torvik, for his sincere guidance and concern during the entire course of this investigation. I am grateful to Dr. Vipperla B. Venkayya and Dr. Donald B. Paul for the expertise that they generously gave in their respective fields of structural analysis and heat transfer. I wish to express my appreciation for the assistance provided by Victoria A. Tischler. In addition, I would like to thank Damaris A. Frantz for her understanding, patience and dedication in typing this report. And finally, I wish to thank my husband Terry and my son Jeremy, for their support and understanding throughout the time I worked on this report.

Sheryl K. Bryan

DTIC
COPY
INSPECTED
3

Accession For		
NTIS GRA&I	✓	
DTIC TAB	☐	
Unannounced	☐	
Justification		
By		
Distribution/		
Availability Codes		
Dist	Avail and/or Special	
A-1		

Contents

List of Figures iv

List of Tables vi

List of Symbols vii

Abstract xi

I.   Introduction 1

II.   Modeling the Structure 4

        Finite Element Method 4
        Finite Elements 10
            Rod Element 13
            Triangular Membrane 16
            Quadrilateral Membrane 24
            Shear Panel 28
        Numerical Solution 30
        Reanalysis Techniques 35
        Estimation of the Effects of Yielding 38
        Convergence Criterion 45

III. Modeling the Thermal Effects 48

        Heat Conduction Problem 48
        Numerical Solution 50
        Melt Calculations 54
        Laser Flux Profile 55
        Results of the Temperature Distribution 56

IV.   Modeling the Damage 61

        Damage Due to Material Loss 61
        Addition of Thermal Loads 65
        Temperature Dependence of Young's Modulus 68

V.   Results 71

        Flat Plate 71
        Intermediate Complexity Wing 86

VI.   Conclusions and Recommendations 99

        Conclusions 99
        Recommendations 99

List of Figures

List of Tables

List of Symbols

Symbol	Definition	Typical Units
$\underset{\sim}{a}$	transformation matrix	dimensionless
$\underset{\sim}{A}$	element geometry matrix	in
A	area	in^2
$\underset{\sim}{B}$	differential operator	dimensionless
c	undetermined coefficients	dimensionless
C_p	specific heat	Btu/lbm °F
$\underset{\sim}{D}$	nodal displacement vector in the global coordinate system	in
$\underset{\sim}{E}$	material property matrix	lbf/in^2
E	Young's modulus	lbf/in^2
$\underset{\sim}{f}$	element displacements in the local coordinate system	in
F_o	peak intensity	Btu/in^2
F	rate of absorbed energy	Btu
$\underset{\sim}{F}$	body forces	lbf/in^2
g	implicit parameter describing stiffness change	dimensionless
h	thickness	in
k	thermal conductivity	Btu/sec in °F
$\underset{\sim}{k}$	element stiffness matrix in the local coordinate system	lbf/in
$\underset{\sim}{K}$	structural stiffness matrix in the global coordinate system	lbf/in
L	length	in
$\underset{\sim}{L}$	unit lower triangular matrix	
$\underset{\sim}{M}$	diagonal matrix	
M	mass	lbm

Symbol	Definition	Typical Units
N_C	number of thickness divisions	dimensionless
N_R	number of radial divisions	dimensionless
$\underline{N}$	shape function	
$\underline{p}$	element nodal forces in the local coordinate system	lbf
$\underline{P}$	structural nodal forces in the global coordinate system	lbf
Q	heat transfer rate	Btu/in^2 sec
r	radius	in
t	thickness	in
T	temperature	°F
T_{melt}	melting temperature	°R, °K
T_o	initial temperature	°R, °K
u	nodal displacements in the local coordinate system (x-direction)	in
U	strain energy	BTU
v	nodal displacements in the local coordinate system (y-direction)	in
V	volume	in^3
x	x-direction coordinate	in
X	stress limit in the x direction	lbf/in^2
y	y-direction coordinate	in
Y	stress limit in the y direction	lbf/in^2
$\underline{Y}$	intermediate matrix	
z	z-direction coordinate	in
Z	stress limit in the z direction	lbf/in^2
α	diffusivity	in^2/sec

Symbol	Definition	Typical Units
Γ	heat of fusion	Btu/lbm
Υ	energy to melt	Btu/lbm
Δ	denotes a change	dimensionless
$\underline{\varepsilon}$	strain	in/in
$\underline{\varepsilon}^{o}$	thermal strain	in/in
η	reduction factor for Young's modulus	dimensionless
Θ	Von Mises criterion	dimensionless
λ	linear percent of load	dimension.
Λ	potential energy of the applied loads	BTU
μ	nonlinear percent of load	dimension
ν	Poison's ratio	in/in
Π	potential energy	BTU
ρ	density	lbm/in^3
σ	half beam radius	in
$\underline{\sigma}$	stress	lbf/in^2
τ	time	sec
ϕ	convergence variable	
$\underline{\psi}$	nodal thermal loads in the local coordinate system	lbf
$\underline{\Psi}$	nodal thermal loads in the global coordinate system	lbf

Superscripts

q	iteration cycle	
s	current value	
T	matrix transpose	
λ	within the linear range	

Symbol	Definition	Typical Units
μ	past the linear range	
-1	matrix inverse	
$\char94$	partitioned component of a matrix	
$*$	denotes a damaged case	
$\sim$	denotes a vector or a matrix	

Subscripts

e	denotes fictious node
i	element designator
i,j	row i, column j
max	maximum
p	denotes a total for the entire structure
Q	references five noded element
r	denotes existing node
R	denotes radial direction
Z	denotes thickness direction

Abstract

A reanalysis method to analyze the strength of a structure which
has encountered a laser strike is developed. The method accounts for
the following types of laser induced damage: 1) loss of structure due
to melting; 2) change of material properties due to temperature changes;
3) addition of load due to thermal stress. The program uses heat
balance calculations over successive finite time increments on an array
of finite elements bisecting the laser beam spot to determine the tem-
perature distribution. These results are then converted to structural
stiffness parameters and the structural analysis is performed using a
finite element based reanalysis method. The reanalysis method predicts
the damage effects from the initial undamaged solution. The program
was found to give good results consistent with results obtained from
a separate analysis for each damage condition, but with less computer
time and manhours.

REANALYSIS METHODS FOR STRUCTURES
WITH LASER INDUCED DAMAGE

I   Int ,:luction

With the current thrust towards laser technology in the development

of weapons, methods must be developed for analyzing the damage due to

lasers. The total problem is a merging of two separate technologies.

The first is the characterization of laser damage. The thermal problem

occurring in the area local to the beam must be related to such concepts

as stiffness which are required for a structural analysis. The second

is the area of structural analysis. A cost effective method for per-

forming the structural analyses necessary for analyzing each damage case

must be developed.

Laser damage studies have been conducted to calculate the tempera-

ture distributions and "melt-through time" for specific conditions

(Ref 1-4). The primary interest of these studies was to determine the

material degradation in the immediate vicinity of the beam spot. The

object of the present study is to relate these local damage mechanisms

to a set of global variables which can be used in a structural analysis.

Depending on which aircraft structural systems are affected and the

degree of the damage, the effect on the performance of a damaged air-

craft can vary from minor changes to the loss of the aircraft. Since

military aircraft are expected to encounter damage, it is important that

they retain some level of structural integrity. This must be provided

for during the design phase. A simplistic approach might be to increase

the sizes of all members and components which make up the structure.

However, the constant quest to reduce weight and cost while increasing

performance through optimization is at odds with such an approach, unless limited to a minimum increase of critical members. The problem lies in determining the location of the critical members, for it is impossible to predict in advance the degree and location of the damage. Thus an analysis must be conducted, investigating a large number of possible levels and locations of damage to identify the areas needing modification. Repeating a complete structural analysis for each hypothetical damage case would be extremely costly.

Recent studies have developed iterative methods to reduce the cost of the large numbers of analyses (Ref 5-9). Such techniques have also been used to analyze the effects of conventional weapons (Ref 9). The object of the present study is to modify and extend the reanalysis iteration technique developed by Venkayya (Ref 5) to allow for efficient analysis of a structure subject to many different damage conditions, and to apply this methodology to the analysis of laser damage.

Combining the objectives of the two merging technologies, the total program objective is to develop a method by which a structural designer can determine critical members of the structure needing strengthening or redundancy to survive laser strikes at relatively low cost. This paper follows the logical development of the program: Section II discusses the structural analysis method to be used and develops the iterative re-analysis technique to be applied to the damaged structure. Section III presents the solution to the heat conduction problem resulting from the laser engagement and provides a means of evaluating the local damage. Section IV develops the relationships necessary to convert the local damage arising from laser heating to damage parameters consistent with the overall structural analysis. Finally, Section V discusses the

results obtained, and Section VI presents conclusions and recommendations for further study.

II Modeling the Structure

The structural analysis method used is based on the displacement method of finite element analysis (Ref 10, 11, and 12). In such an analysis, the continuum is replaced by a discrete model consisting of a finite number of elements connected at nodes (See Figure 1). The rationale in such an approximation is that the response between the nodes, i.e., the response in the elements, can be expressed as a function of the response at the nodes. Various interpolation functions or shape functions are used to determine the element response from the nodal response. The type of function used depends on the complexity of response allowed for each element. The discretization reduces the original differential equations of the continuum to a set of algebraic equations which can be readily solved on digital computers. The iterative reanalysis technique employs the original analysis of the undamaged structure. Therefore the development of the reanalysis technique will also include the development of the basic steps of the displacement method for finite element analysis.

The finite element method used in this study is based on the generalized displacement method. The computer program used is a modification of the program "ANALYZE" (Ref 12) which was originally developed for in-house studies in structural analysis and optimization at the Flight Dynamics Laboratory, Wright-Patterson AFB.

Finite Element Method

The following derivation parallels a standard development for the finite element method (Ref 10, 11, 12). The finite element method was derived through variational calculus using the principle of minimum
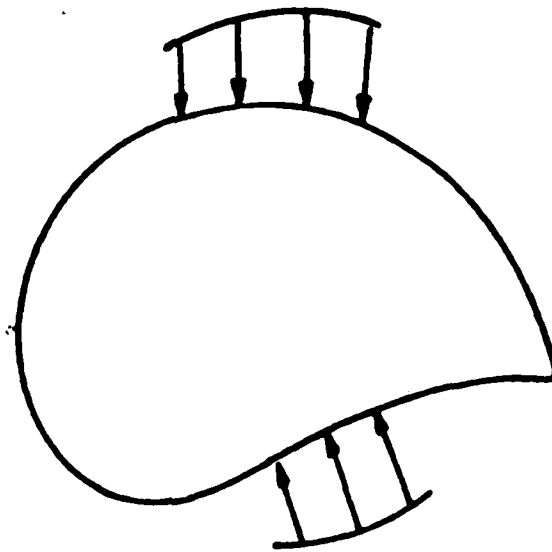
(a) Continuum
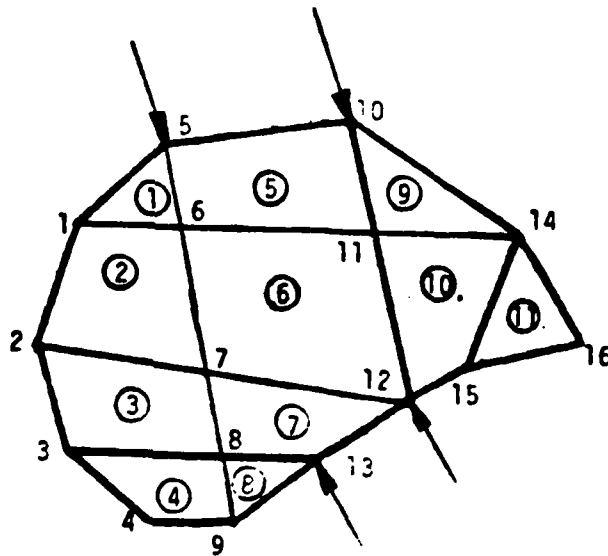
(b) Finite Element Model

Figure 1.   Finite Element Approximation

5

potential energy as the starting point. The potential energy, Π_p, of a structure is defined as (Ref 11:153)

$$\Pi_p = U + \Lambda \tag{1}$$

where U is the strain energy and Λ is the potential of the applied loads. The principle of minimum potential energy can be stated as follows: "Among all displacements of an admissible form, those that satisfy the equilibrium conditions make the potential energy assume a stationary value. Thus

$$\delta\Pi_p = \delta U + \delta\Lambda = 0 \tag{2}$$

For stable equilibrium Π_p is a minimum. Hence

$$\delta^2\Pi_p = \delta^2 U + \delta^2\Lambda > 0 \tag{3}$$

Displacements of an admissible form are defined as those satisfying internal compatibility and kinematic boundary conditions (Ref 10:56).

For a discrete finite element model the total potential energy is a sum of the functionals for each element (Π_i), i.e.,

$$\Pi_p = \sum_{i=1}^{n} \Pi_i = \sum_{i=1}^{n} (U_i + \Lambda_i) \tag{4}$$

where n is the number of elements. The equations for finite element analysis can then be derived from the element equations. If the structure is modeled by n finite elements connecting m nodes, the strain energy of the ith element is

$$U_i = \frac{1}{2} \int_{V_i} \sigma_i^T \varepsilon_i \, dV \tag{5}$$

6

where σ_i^T is the transpose of the stress vector, ε_i is the strain vector and V_i is the volume of the element. From Hooke's Law the stress-strain relationship for a linearly elastic body can be written as

$$\sigma_i = E_i \varepsilon_i \tag{6}$$

where E_i is the symmetric material-stiffness matrix. For the typical homogeneous, isotropic plane stress element E_i is defined by

$$E_i = \frac{E_i}{1-\nu_i^2} \begin{bmatrix} 1 & \nu_i & 0 \\ \nu_i & 1 & 0 \\ 0 & 0 & \frac{1}{2}(1-\nu_i) \end{bmatrix} \tag{7}$$

where E_i is Young's modulus of elasticity and ν_i is Poisson's ratio.

The finite element approximation is based on the assumption that the displacements within an element can be adequately described by simple polynomials. The coefficients of the polynomials in turn are related to the discrete nodal displacements of the element. Therefore, the internal displacement equation is a vector equation of the form

$$f_i = N_i u_i \tag{8}$$

where f_i is the vector of displacements in the element coordinate system, N_i is the interpolation or shape function and u_i are the nodal displacements.

The strain - displacement relations can be written as

$$\varepsilon_i = B f_i \tag{9}$$

where B is a linear differential operator. For the general problem B is defined as

7

$$B = \begin{bmatrix} \frac{\partial}{\partial x} & 0 & 0 \\[1.2em] 0 & \frac{\partial}{\partial y} & 0 \\[1.2em] 0 & 0 & \frac{\partial}{\partial z} \\[1.2em] \frac{\partial}{\partial y} & \frac{\partial}{\partial x} & 0 \\[1.2em] 0 & \frac{\partial}{\partial z} & \frac{\partial}{\partial y} \\[1.2em] \frac{\partial}{\partial z} & 0 & \frac{\partial}{\partial x} \end{bmatrix} \qquad (10)$$

Substituting Equations 6, 8 and 9 into Equation 5 gives the following expression for the element strain energy,

$$U_i = \frac{1}{2} \int_{V_i} u_i^T N_i^T B_i^T E_i B_i N_i u_i \, dV \qquad (11)$$

At this point the basic finite element assumption, i.e., that the internal element displacements are a function of the nodal displacements, makes its major impact on the analysis. Through this assumption the nodal displacements have been made independent of the integration in space because they represent displacements at specific locations. Therefore, the u_i can be taken out of the integral as follows

$$U_i = \frac{1}{2} u_i^T \int_{V_i} N_i^T B_i^T E_i B_i N_i \, dV \, u_i \qquad (12)$$

The elemental stiffness matrix, $\underline{k}_i$, is defined as

$$\underline{k}_i = \int_{V_i} \underline{N}_i^T \underline{B}_i^T \underline{E}_i \underline{B}_i \underline{N}_i \, dV \tag{13}$$

Equation 12 can be written as

$$U_i = \frac{1}{2} \underline{u}_i^T \underline{k}_i \underline{u}_i \tag{14}$$

The potential of the applied loads is given by

$$\Lambda_i = -\int \underline{u}_i^T \underline{F}_i \, dV - \underline{u}_i^T \underline{p}_i \tag{15}$$

where $\underline{F}_i$ is the vector of lumped body forces per unit volume and $\underline{p}_i$ is the vector of nodal forces. The sign is negative because applied loads lose potential when displacement takes place. This analysis assumes that the body forces are zero allowing only nodal forces. Thus Equation 15 can be written as

$$\Lambda_i = - \underline{u}_i^T \underline{p}_i \tag{16}$$

Substituting Equations 14 and 16 into Equation 4 gives the following expression for the potential energy

$$\pi_p = \sum_{i=1}^{n} \left(\frac{1}{2} \underline{u}_i^T \underline{k}_i \underline{u}_i - \underline{u}_i^T \underline{p}_i \right) \tag{17}$$

At this point, there are n expressions which must be summed to calculate the potential energy of the entire structure. However, each expression is measured in the local coordinate system of the corresponding element. In order to combine the element expressions into a single structural equation, a transformation matrix, $\underline{a}_i$, is introduced such that

$$U_i = a_i D \tag{18}$$

where D is the structural displacement vector in the global coordinate system. Substituting Equation 18 into 17 gives

$$\Pi_p = \sum_{i=1}^{n} (\frac{1}{2} D^T a_i^T k_i a_i D - D^T a_i^T p_i) \tag{19}$$

Since D is independent of i it can be pulled outside the summation. Then letting

$$K = \sum_{i=1}^{n} a_i^T k_i a_i$$

and $\hspace{10cm}$ (20)

$$P = \sum_{i=1}^{n} a_i^T p_i$$

where K is the total structural stiffness matrix and P is the total structural load matrix, Equation 19 becomes

$$\Pi_p = \frac{1}{2} D^T K D - D^T P \tag{21}$$

Taking the first variation with respect to the displacements gives

$$\begin{aligned} \delta\Pi_p &= \delta(\frac{1}{2} D^T K D) - \delta(D^T P) \\ &= \delta D^T K D - \delta D^T P \\ &= \delta D^T (K D - P) \end{aligned} \tag{22}$$

10

The principle of minimum potential energy, Equation 2, requires that

$$\underline{K}\underline{D} - \underline{P} = 0 \tag{23}$$

Equation 23 is a set of algebraic equations, which may be solved numerically. Once the displacements are found from the solution of Equation 23, the internal displacements, strains and stresses can be determined by Equations 18, 8, 9 and 6.

Finite Elements

The finite element program used for this analysis contains four basic elements. They are the (1) rod, (2) membrane triangle, (3) membrane quadrilateral and (4) shear panel. The rod elements have constant cross-sectional areas, and the planar elements have constant thicknesses. The nodal displacement vectors are shown in Figure 2 for each element. The rod is a constant strain line element allowing only axial displacements. The membrane triangle is a constant strain planar element, and the membrane quadrilateral is constructed out of four nonoverlapping constant strain triangles using a fictitious interior node that is removed using static condensation. The process of static condensation will be discussed in the Quadrilateral Membrane Subsection. Construction of the shear panel element is similar to the membrane quadrilateral using four nonoverlapping triangles. However, only the shear strains are included in the element stiffness matrix computation. In general, these four elements are adequate for determining the primary load paths in most aircraft structures such as wings and fuselages. However, more complex elements may be needed for a detailed stress analysis of local areas.
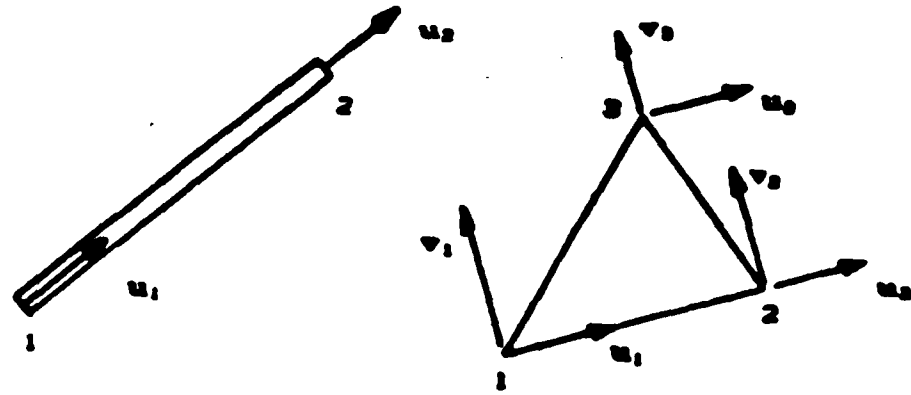
(a) Bar Element　　　　(b) Triangular Membrane Element
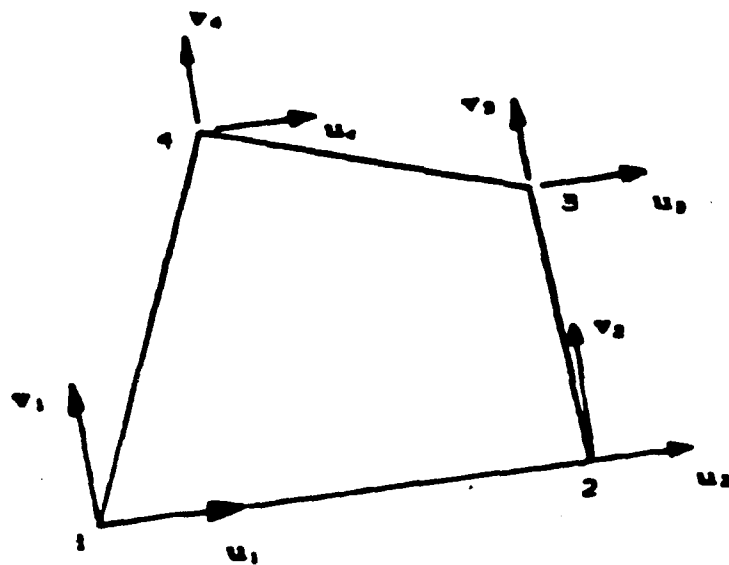
(c) Quadrilateral or Shear Panel

Figure 2.　Elements and Local Coordinate System

Rod Element

The rod element is an axial force member commonly seen as a section in an analysis of a two or three dimensional truss structure. However, within an aircraft structure, it is used to model spar and rib caps. Figure 2a shows the allowable nodal displacements as defined by the local coordinate system. The positive x-axis is defined as being directed along the line from the first node to the second. The rod is a two degree of freedom element since its element displacement vector has two components u_1 and u_2.

Since the rod is defined as a constant strain element, the internal displacements are assumed to be linear and can be approximated by a linear function

$$f = c_1 + c_2 x = \begin{bmatrix} 1 & x \end{bmatrix} \begin{bmatrix} c_1 \\ c_2 \end{bmatrix} = \underline{x} \underline{c} \tag{24}$$

where f is the internal displacement at the location x, and the c's are coefficients to be determined. For a linear elastic material, the stress in the element will also be constant.

Applying the boundary conditions

$$\begin{aligned} f &= u_1 \text{ at } x = 0 \\ f &= u_2 \text{ at } x = L \end{aligned} \tag{25}$$

one obtains

$$u_1 = c_1 \tag{26}$$

$$u_2 = c_1 + c_2 L$$

13

If one lets

$$\underline{u} = \begin{bmatrix} u_1 \\ u_2 \end{bmatrix}$$

$$\underline{A} = \begin{bmatrix} 1 & 0 \\ 1 & L \end{bmatrix}$$

(27)

and

$$\underline{c} = \begin{bmatrix} c_1 \\ c_2 \end{bmatrix}$$

then Equation 26 can be written in matrix form as

$$\underline{u} = \underline{A}\underline{c}$$ (28)

Solving for the coefficient vector

$$\underline{c} = \underline{A}^{-1}\underline{u}$$ (29)

and substituting into Equation 24 gives

$$f = \underline{x}\underline{A}^{-1}\underline{u}$$ (30)

Then

$$\underline{N} = \underline{x}\underline{A}^{-1} = \begin{bmatrix} \dfrac{L-x}{L} & \dfrac{x}{L} \end{bmatrix}$$ (31)

14

where $\underline{N}$ is the shape function describing the linear relationship between the internal and nodal displacements (See Equation 8).

The strain - displacement relation for axial strain can be written as

$$\varepsilon_x = \frac{\partial f}{\partial x}$$

(32)

Therefore $\underline{B}$, as defined in Equation 9, takes the form

$$\underline{B} = \begin{bmatrix} \frac{\partial}{\partial x} \\ 0 \end{bmatrix}$$

(33)

for the axial rod element.

For the rod element the stress-strain relationship is simply

$$\sigma = E\varepsilon$$

(34)

Substituting Equations 30, 33, and 34 into Equation 13 gives

$$k_i = \int_{V_i} \begin{bmatrix} \frac{L-x}{L} \\ \frac{x}{L} \end{bmatrix} \begin{bmatrix} \frac{\partial}{\partial x} & 0 \end{bmatrix} E_i \begin{bmatrix} \frac{\partial}{\partial x} \\ 0 \end{bmatrix} \begin{bmatrix} \frac{L-x}{L} & \frac{x}{L} \end{bmatrix} dV$$

$$= \frac{E_i}{L_i^2} \begin{bmatrix} 1 & -1 \\ -1 & 1 \end{bmatrix} \int_{V_i} dV$$

(35)

Since

$$A_i L_i = \int_{V_i} dV \qquad (36)$$

where A is the cross sectional area and L is the length of the rod, Equation 13 takes the form

$$\underline{k}_i = \frac{A_i E_i}{L_i} \begin{bmatrix} 1 & -1 \\ -1 & 1 \end{bmatrix} \qquad (37)$$

for the rod element.

Triangular Membrane

The basic planar element in this program is the membrane triangle. It is also used in the construction of the quadrilateral membrane and the shear panel. Since it is a plane stress element, it can be used effectively where the primary loading is in-plane forces, i.e., the top and bottom skin of aircraft wings, flanges of I and box beams subjected to constant normal stresses, and the skins of sandwich composite construction. However, this element is not suitable when the stresses through the thickness vary significantly (plate bending). Inappropriate use of this element will overestimate the stiffness or generate a matrix singularity. Figure 2b shows the allowable nodal displacements as defined by the local coordinate system. The internal displacements are assumed to be linear in x and y and can be represented by

$$f_x = c_1 + c_2 x + c_3 y$$

$$f_y = c_4 + c_5 x + c_6 y$$

(38)

where f_x and f_y are the x and y displacements in the plane of the plate measured in the local coordinate system at location (x,y) and the c's are the coefficients to be determined. Equation 38 can be written in matrix form as

$$\underline{f} = \underline{x}\,\underline{c}$$

(39)

where

$$\underline{f} = \begin{bmatrix} f_x \\ f_y \end{bmatrix}$$

$$x = \begin{bmatrix} 1 & x & y & 0 & 0 & 0 \\ 0 & 0 & 0 & 1 & x & y \end{bmatrix}$$

17

and

$$\mathcal{C} = \begin{bmatrix} c_1 \\ c_2 \\ c_3 \\ c_4 \\ c_5 \\ c_6 \end{bmatrix}$$

Since the locations of the nodes are within the domain of the element, the boundary conditions are

$$u_1 = c_1 + c_2 x_1 + c_3 y_1$$
$$v_1 = c_4 + c_5 x_1 + c_6 y_1$$
$$u_2 = c_1 + c_2 x_2 + c_3 y_2$$
$$v_2 = c_4 + c_5 x_2 + c_6 y_2 \qquad (40)$$
$$u_3 = c_1 + c_2 x_3 + c_3 y_3$$
$$v_3 = c_4 + c_5 x_3 + c_6 y_3$$

where the u_i and v_i are the x and y displacements of the ith node at location (x_i, y_i) (See Figure 2b). Regrouping Equations 40 and re-writing in matrix notation gives the nodal displacement equations in the form

$$
\underline{u} = \begin{bmatrix} u_1 \\ u_1 \\ u_3 \\ - \\ v_1 \\ v_2 \\ v_3 \end{bmatrix} = \begin{bmatrix} 1 & x_1 & y_1 & 0 & 0 & 0 \\ 1 & x_2 & y_2 & 0 & 0 & 0 \\ 1 & x_3 & y_3 & 0 & 0 & 0 \\ - & - & - & + & - & - & - \\ 0 & 0 & 0 & 1 & x_1 & y_1 \\ 0 & 0 & 0 & 1 & x_2 & y_2 \\ 0 & 0 & 0 & 1 & x_3 & y_3 \end{bmatrix} \begin{bmatrix} c_1 \\ c_2 \\ c_3 \\ c_4 \\ c_5 \\ c_6 \end{bmatrix} \tag{41}
$$

Note that the nodal coordinate matrix on the right hand side partitions into a diagonal matrix. Since the construction of the x and y coefficients is identical, the inversion of the partitioned diagonal matrix is simply the inversion of the component matrix. In matrix form Equation 41 becomes

$$
\underline{u} = \begin{bmatrix} \underline{A} & 0 \\ - & + & - \\ 0 & \underline{A} \end{bmatrix} \underline{c}
$$

19

with the solution in the form

$$
\underline{c} = \begin{bmatrix} \hat{A}^{-1} & \vline & 0 \\ - & - \vline - & - \\ 0 & \vline & \hat{A}^{-1} \end{bmatrix} \underline{u}
$$

For simplicity, only the derivation of x direction coefficients will be shown and use of the ^ notation will represent the x direction component of the partitioned matrix. Thus Equation 41 simplifies to

$$
\hat{\underline{u}} = \begin{bmatrix} u_1 \\ u_2 \\ u_3 \end{bmatrix} = \begin{bmatrix} 1 & x_1 & y_1 \\ 1 & x_2 & y_2 \\ 1 & x_3 & y_3 \end{bmatrix} \begin{bmatrix} c_1 \\ c_2 \\ c_3 \end{bmatrix} = \hat{A} \; \hat{\underline{c}}
\tag{42}
$$

which has the same form as Equation 28 for the rod element. Solving for the coefficient vector

$$
\hat{\underline{c}} = \frac{1}{\det|\hat{A}|} \begin{bmatrix} x_2 y_3 - x_3 y_2 & x_3 y_1 - x_1 y_3 & x_1 y_2 - x_2 y_1 \\ y_2 - y_3 & y_3 - y_1 & y_1 - y_2 \\ x_3 - x_2 & x_1 - x_3 & x_2 - x_1 \end{bmatrix} \begin{bmatrix} u_1 \\ u_2 \\ u_3 \end{bmatrix}
\tag{43}
$$

and substituting into Equation 39 gives

$$\hat{\underline{f}} = \hat{\underline{x}}\underline{A}^{-1}\hat{\underline{u}} \qquad (44)$$

Then

$$\underline{N} = \hat{\underline{x}}\underline{A}^{-1} = \frac{1}{\det|A|}\begin{bmatrix} x_2y_3 - x_3y_2 + x(y_2 - y_3) + y(x_3 - x_2), \\ x_3y_1 - x_1y_3 + x(y_3 - y_1) + y(x_1 - x_3), \\ x_1y_2 - x_2y_1 + x(y_1 - y_2) + y(x_2 - x_1) \end{bmatrix} \qquad (45)$$

where $\underline{N}$ is the shape function describing the linear relationship between the internal and nodal displacements. Expanding the solution to include the x and y displacements gives

$$\underline{f} = \begin{bmatrix} N_1 & N_2 & N_3 & 0 & 0 & 0 \\ 0 & 0 & 0 & N_1 & N_2 & N_3 \end{bmatrix} \underline{u} \qquad (46)$$

where N_i is the ith element of $\underline{N}$ as given in Equation 45 and $\underline{u}$ is the nodal displacement vector as defined in Equation 41. Standard practice groups the nodal displacements by node rather than direction, therefore regrouping Equation 46 gives

$$\underline{f} = \begin{bmatrix} N_1 & 0 & N_2 & 0 & N_3 & 0 \\ 0 & N_1 & 0 & N_2 & 0 & N_3 \end{bmatrix} \underline{u} \qquad (47)$$

where

$$\underset{\sim}{u} = \begin{bmatrix} u_1 \\ v_1 \\ u_2 \\ v_2 \\ u_3 \\ v_3 \end{bmatrix}$$

Using the plane stress assumption, the differential operator $\underset{\sim}{B}$ as defined by the strain displacement relations in Equation 9 reduces to

$$\underset{\sim}{B} = \begin{bmatrix} \dfrac{\partial}{\partial x} & 0 \\ 0 & \dfrac{\partial}{\partial y} \\ \dfrac{\partial}{\partial y} & \dfrac{\partial}{\partial x} \end{bmatrix} \tag{48}$$

which when applied to $\underset{\sim}{N}$ yields only constants. The differential volume is $dV_i = t_i dA_i$ where t_i is the constant thickness and A_i is the area of the element. $\underset{\sim}{E}_i$ is constant as defined by Equation 7. Therefore,

22

Equation 13 yields

$$k_i = N_i^T B_i^T E_i B_i N_i t_i A_i \tag{49}$$

Substituting Equations 7, 45 and 48 into Equation 49 gives

$$k_i = \frac{E_i t_i}{4A_i(1-\nu_i^2)} \begin{bmatrix}
y_{32}^2 + x_{32}^2 \frac{(1-\nu)}{2} & & \text{Symmetric} \\
-(\nu y_{32} x_{32} + x_{32} y_{32} \frac{(1-\nu)}{2}) & x_{32}^2 + y_{32}^2 \frac{(1-\nu)}{2}, & \\
-(y_{32} y_{31} + x_{32} x_{31} \frac{(1-\nu)}{2}) & (\nu x_{32} y_{31} + y_{32} x_{31} \frac{(1-\nu)}{2}), & \\
(\nu y_{32} x_{31} + x_{32} y_{31} \frac{(1-\nu)}{2}) & -(x_{32} x_{31} + y_{32} y_{31} \frac{(1-\nu)}{2}), & \\
(y_{32} y_{21} + x_{32} x_{21} \frac{(1-\nu)}{2}) & -(\nu x_{32} y_{21} + y_{32} x_{21} \frac{(1-\nu)}{2}), & \\
-(\nu y_{32} x_{21} + x_{32} y_{21} \frac{(1-\nu)}{2}) & (x_{32} x_{21} + y_{32} y_{21} \frac{(1-\nu)}{2}),
\end{bmatrix}$$

$$\begin{aligned}
&y_{31}^2 + x_{31}^2 \frac{(1-\nu)}{2}, \tag{50} \\
&-(\nu y_{31} x_{31} + x_{31} y_{31} \frac{(1-\nu)}{2}) \quad x_{31}^2 + y_{31}^2 \frac{(1-\nu)}{2}, \\
&-(y_{31} y_{21} + x_{31} x_{21} \frac{(1-\nu)}{2}) \quad (\nu x_{31} y_{21} + y_{31} x_{21} \frac{(1-\nu)}{2}), \\
&(\nu y_{31} x_{21} + x_{31} y_{21} \frac{(1-\nu)}{2}) \quad -(x_{31} y_{21} + y_{31} x_{21} \frac{(1-\nu)}{2}),
\end{aligned}$$

$$\begin{aligned}
&y_{21}^2 + x_{21}^2 \frac{(1-\nu)}{2} \\
&-(\nu y_{21} x_{21} + x_{21} y_{21} \frac{(1-\nu)}{2}) \quad x_{21}^2 + y_{21}^2 \frac{(1-\nu)}{2}
\end{aligned}$$

where $\underline{k}_i$ is the element stiffness matrix for a triangular membrane element and $x_{ij} = x_i - x_j$ and $y_{ij} = y_i - y_j$.
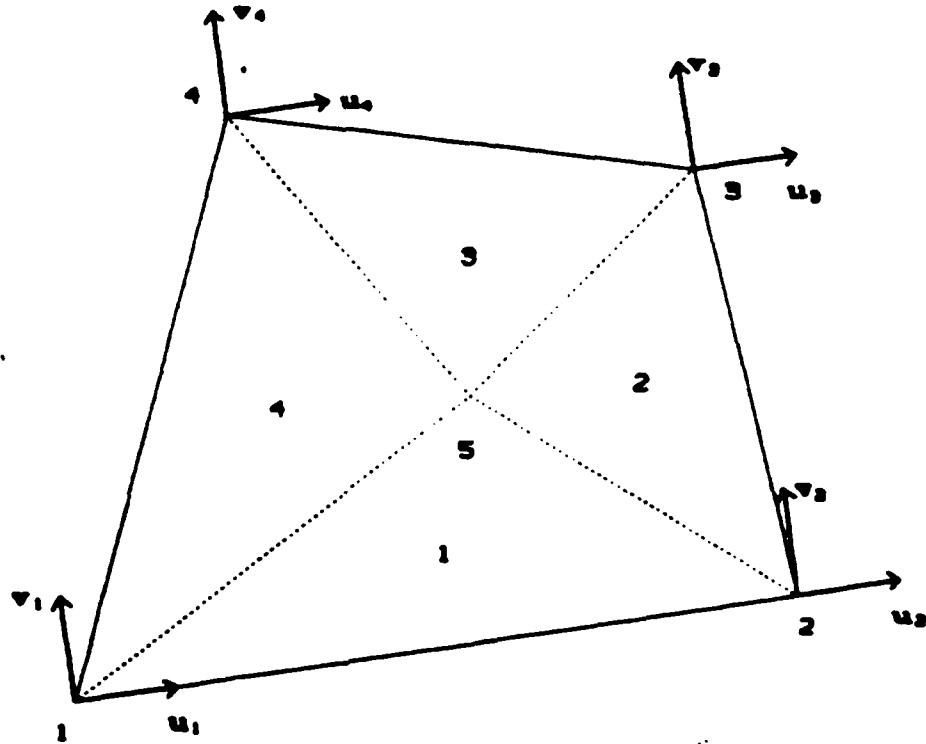
Quadrilateral Membrane

The quadrilateral membrane is the element most often used to represent structural skins because large areas with minimal curvature can easily be represented by four-sided planes. Figure 2c shows the allowable nodal displacements as defined by the local coordinate system. The element is assumed to be a plane defined by the first three nodes. This assumption ignores all warping and will result in an overestimation of the stiffness if out of plane warping is significant. However, this element can be used in regions of high warping if the sizes of the elements are reduced appropriately.

The stiffness of the quadrilateral membrane is constructed by dividing it into four triangular membranes. As shown in Figure 3, a fictitious fifth node is required and is located by averaging the coordinates of the element's four actual nodes using the expressions

$$x_5 = \frac{x_1 + x_2 + x_3 + x_4}{4}$$

$$y_5 = \frac{y_1 + y_2 + y_3 + y_4}{4}$$

This subdivision improves the accuracy of the quadrilateral element by using more nodal displacements without burdening the user with the task of defining them. A stiffness matrix, $\hat{k}_i$, is computed for each of the four triangular elements using Equation 50. Then the addition of the four matrices is accomplished, similar to the summation of the element matrices described in Equations 18 and 20. A transformation matrix, $\hat{a}_i$, is introduced such that

Figure 3. Quadrilateral or Shear Panel
Divided into Four Triangles

$$\hat{\underline{u}}_i = \hat{\underline{a}}_i \underline{u}_Q \tag{51}$$

where $\underline{u}_Q$ is the nodal displacement vector for the five node quadrilateral element, and $\underline{u}_i$ is the nodal displacement vector for the ith triangular membrane. Each triangular stiffness matrix is then transformed and their summation results in the following expression

$$\underline{k}_Q = \sum_{i=1}^{4} \hat{\underline{a}}_i^T \hat{\underline{k}}_i \hat{\underline{a}}_i \tag{52}$$

where $\underline{k}_Q$ is the 10 x 10 stiffness matrix for the five node quadrilateral which includes terms for the nodal displacements of the fictitious node. The fictitious node's displacements are removed using the following static condensation procedure - a manipulation of the stiffness matrix, not an approximation.

The equilibrium equation for the five node quadrilateral can be written as

$$\underline{k}_Q \underline{u}_Q = \underline{p}_Q \tag{53}$$

where $\underline{p}_Q$ is the vector of applied nodal forces. Partitioning Equation 53 such that

$$\underline{u}_Q = \begin{bmatrix} \underline{u}_r \\ \hline \underline{u}_e \end{bmatrix} \tag{54}$$

where $\underline{u}_r$ are the nodal displacements for the original four nodes to be retained and $\underline{u}_e$ are those for the fictitious node to be eliminated gives

$$\begin{bmatrix} k_{rr} & | & k_{re} \\ - & - & - \\ k_{er} & | & k_{ee} \end{bmatrix} \begin{bmatrix} \underline{u}_r \\ - \\ \underline{u}_e \end{bmatrix} = \begin{bmatrix} \underline{p}_r \\ - \\ \underline{p}_e \end{bmatrix} \qquad (55)$$

which can be expressed as two separate equations

$$\underline{k}_{rr}\underline{u}_r + \underline{k}_{re}\underline{u}_e = \underline{p}_r \qquad (56)$$

and

$$\underline{k}_{er}\underline{u}_r + \underline{k}_{ee}\underline{u}_e = \underline{p}_e \qquad (57)$$

Since the p_i are the given nodal forces and the fifth node is not actually present in the original model, the forces on this node are zero. Therefore, the partition of p containing the nodal forces applied to the fifth node, $\underline{p}_e$, must be zero. Using this condition and solving Equation 57 for $\underline{u}_e$ gives

$$\underline{u}_e = - \underline{k}_{ee}^{-1}\underline{k}_{er}\underline{u}_r \qquad (58)$$

Equation 56 can now be written as

$$\underline{k}_{rr}\underline{u}_r + \underline{k}_{re}(- \underline{k}_{ee}^{-1}\underline{k}_{er}\underline{u}_r) = \underline{p}_r$$

or

$$(\underline{k}_{rr} - \underline{k}_{re}\underline{k}_{ee}^{-1}\underline{k}_{er})\underline{u}_r = \underline{p}_r$$

(59)

27

Note that Equation 59 has the same form as Equation 23, i.e., Equation 59 is the equilibrium equation for the original quadrilateral membrane. Thus, the element stiffness matrix, $\underset{\sim}{k}$, can be written

$$\underset{\sim}{k}_i = (\underset{\sim}{k}_{rr} - \underset{\sim}{k}_{re}\underset{\sim}{k}_{ee}^{-1}\underset{\sim}{k}_{er}) \tag{60}$$

Shear Panel

The shear panel is a constant shear stress element and cannot carry normal stresses. It was a common practice, prior to the development of the finite element method, to model wing, fuselage and empennage structures with constant shear panels surrounded by rod elements carrying the normal stresses. With the development of finite element methods and the quadrilateral membrane, the top and bottom skins were more easily modeled using membrane elements, since they required the definition of nodes and connectivity of a single element rather than the definition of five elements needed for the shear panel and rod construction. However, the use of membranes to model spars and webs results in a gross over-estimation of the structural stiffness due to the constant strain assumption. Most spars, ribs and box or I-beam webs carry primarily shear with some normal stress, resulting in deformations due to shear stresses, not normal stresses. In addition, the normal stresses usually have steep stress gradients which, as stated in the development of the membrane triangle, cannot be modeled using a constant strain planar element. Therefore, the shear panel was developed (Ref 13) to accurately model these structural webs without complicating the constant strain membranes. Since the shear panel is assumed to carry only shear stresses, it must be surrounded by rod or membrane elements to carry the normal stresses. Even though the actual structure does not contain

28

normal load members, the user must provide fictitious ones, usually rod elements, or the stiffness matrix will be singular. The use of this idealized model construction has proven to produce accurate results when used with the appropriate loading conditions. For example, when modeling the ribs and spars of a wing, the use of shear panels is appropriate if the major loading condition is lift (Ref 12). However, when drag is the major loading condition shear panels will produce totally erroneous results.

The shear panel is constructed like the quadrilateral membrane by division into four component triangles. However, the stiffness matrices of the triangles are calculated using only the shear strain energy terms. Thus the $\underline{B}$ matrix reduces to

$$\underline{B} = \begin{bmatrix} 0 & 0 \\ 0 & 0 \\ \frac{\partial}{\partial y} & \frac{\partial}{\partial x} \end{bmatrix} \tag{61}$$

which when used in equation 50 produces

$$k_i = \frac{E_i t_i}{8A_i(1+v_i)} \begin{bmatrix} x_{32}^2 & & & & \text{Symmetric} & \\ -x_{32}y_{32} & y_{32}^2 & & & & \\ -x_{32}x_{31} & y_{32}x_{31} & x_{31}^2 & & & \\ x_{32}y_{31} & -y_{32}y_{31} & -x_{31}y_{31} & y_{31}^2 & & \\ x_{32}x_{21} & -y_{32}x_{21} & -x_{31}x_{21} & y_{31}x_{21} & x_{21}^2 & \\ x_{32}y_{21} & y_{32}y_{21} & x_{31}y_{21} & -y_{31}y_{21} & -x_{21}y_{21} & y_{21}^2 \end{bmatrix} \tag{62}$$

where $x_{ij} = x_i - x_j$ and $y_{ij} = y_i - y_j$. The component stiffness matrices are then combined and reduced in the same way as described for the quadrilateral element, Equations 51 through 60.

Note that since the shear stress of an element is dependent on the orientation of the reference axis, the stiffness matrix can also be affected. For rectangular quadrilaterals, the shear stress would be the same regardless of the side selected to determine the reference axis since all sides will produce identical orientations. But, for the general quadrilateral, large differences in the angles at the corners can produce errors. However, by keeping the element shape fairly close to a rectangle, errors will be reduced to an insignificant level.

Numerical Solution

The majority of the computational time for a finite element analysis is spent solving Equation 23. Since the matrix $\underline{K}$ can be quite large, calculating its inverse could be extremely time consuming. Therefore, taking advantage of the fact that the structural stiffness matrix is always symmetric, positive definite and in most cases sparsely populated, the solution can be found economically using Gaussian elimination (Ref 14:87-88). The procedure consists of three basic steps. The first step is a symmetric decomposition of the original stiffness matrix formulated in the following way

$$\underline{K} = \underline{L} \, \underline{M} \, \underline{L}^T$$

(63)

where $\underline{L}$ is a lower unit triangular matrix of the form

$$
\underline{L} = \begin{bmatrix}
1 & 0 & 0 & . & . & . & 0 \\
L_{21} & 1 & 0 & . & . & . & 0 \\
L_{31} & L_{32} & 1 & & & & . \\
L_{41} & L_{42} & L_{43} & 1 & & & . \\
. & . & & . & & & \\
. & . & & & . & & \\
. & . & & & & . & \\
L_{n1} & L_{n2} & & . & . & . & 1
\end{bmatrix}
\tag{64}
$$

and $\underline{M}$ is a diagonal matrix

$$
\underline{M} = \begin{bmatrix}
M_{11} & 0 & 0 & . & . & . & 0 \\
0 & M_{22} & 0 & . & . & . & 0 \\
0 & 0 & M_{33} & & & & \\
. & . & & . & & & . \\
. & . & & & . & & . \\
. & . & & & & . & . \\
0 & 0 & & . & . & . & M_{nn}
\end{bmatrix}
\tag{65}
$$

31

The $\underline{L}$ and $\underline{M}$ matrices can be calculated using the following procedure. Computing the multiplications in Equation 63 gives

$$
\underline{L}\,\underline{M}\,\underline{L}^T = \begin{bmatrix}
M_{11} & & & & & & \text{Symmetric} \\
M_{11}L_{21} & M_{11}L_{21}^2 + M_{22} & & & & & \\
M_{11}L_{31} & M_{11}L_{31}L_{21} + M_{22}L_{32} & & & & & \\
& & M_{11}L_{31}^2 + M_{22}L_{32}^2 + M_{33} & & & \\
\cdot & & & & & \\
\cdot & & & & & \\
\cdot & & & & & \\
M_{11}L_{n1} & & & & \sum_{i=1}^{n} M_{ii}L_{ni}^2
\end{bmatrix}
$$

It follows then from Equation 63 that

$$
M_{11} = K_{11}, \quad L_{21} = \frac{K_{12}}{M_{11}}, \quad \ldots \quad , \quad L_{n1} = \frac{L_{1n}}{M_{11}}
$$

$$
M_{22} = K_{22} - M_{11}L_{21}^2 \ldots \text{ etc}
$$

The advantage of this particular decomposition is that the sparseness characteristic of the stiffness matrix is also found in the $\underline{L}$ matrix. This reduces the number of computations.

Substituting Equation 63 into Equation 23 gives

$$\underline{L} \; \underline{M} \; \underline{L}^T \; \underline{D} = \underline{P} \tag{66}$$

By simply regrouping

$$\underline{L}[\underline{M} \; \underline{L}^T \; \underline{D}] = \underline{P} \tag{67}$$

and letting

$$\underline{Y} = \underline{M} \; \underline{L}^T \; \underline{D} \tag{68}$$

Equation 66 can be written as

$$\underline{L} \; \underline{Y} = \underline{P} \tag{69}$$

The second step is the calculation of the vector $\underline{Y}$ by forward substitution. Rewriting Equation 67 as

$$
\begin{bmatrix}
1 & 0 & 0 & . & . & . & . & 0 \\
L_{21} & 1 & 0 & & & & & \\
L_{31} & L_{32} & 1 & & & . & & \\
. & & & . & & & & \\
. & & & & . & & & \\
. & & & & & . & & \\
L_{n1} & . & . & & . & & & 1
\end{bmatrix}
\begin{bmatrix}
Y_1 \\ Y_2 \\ Y_3 \\ . \\ . \\ . \\ Y_n
\end{bmatrix}
=
\begin{bmatrix}
P_1 \\ P_2 \\ P_3 \\ . \\ . \\ . \\ P_n
\end{bmatrix}
\tag{70}
$$

then

$$Y_1 = P_1$$

$$L_{21}Y_1 + Y_2 = P_2 \qquad\qquad \rightarrow \quad Y_2 = P_2 - L_{21}Y_1$$

$$L_{31}Y_1 + L_{32}Y_2 + Y_3 = P_3 \quad \rightarrow \quad Y_3 = P_3 - L_{31}Y_1 - L_{32}Y_2 \tag{71}$$

$$\vdots$$

$$\text{etc}$$

33

The last step is to solve for the nodal displacement vector $\underline{D}$ in Equation 68. The technique used is backward substitution which is similar to the forward substitution described in Equations 70 and 71. Rewriting Equation 68 as

$$
\begin{bmatrix}
M_{11} & 0 & & 0 & 1 & L_{21} & L_{31} & \cdots & L_{n1} \\
0 & M_{22} & & \cdot & 0 & 1 & L_{32} & & \\
0 & 0 & & \cdot & 0 & 0 & 1 & & \\
\cdot & & & \cdot & \cdot & & & & \\
\cdot & & & \cdot & & & & & \\
\cdot & & & \cdot & & & & & \\
0 & & M_{nn} & 0 & & & & & 1
\end{bmatrix}
\begin{bmatrix}
D_1 \\ D_2 \\ D_3 \\ \cdot \\ \cdot \\ \cdot \\ D_n
\end{bmatrix}
=
\begin{bmatrix}
Y_1 \\ Y_2 \\ Y_3 \\ \cdot \\ \cdot \\ \cdot \\ Y_n
\end{bmatrix}
\tag{72}
$$

then

$$M_{nn}D_n = Y_n \qquad\qquad \rightarrow\quad D_n = \frac{Y_n}{M_{nn}}$$

$$M_{n-1,n-1}D_{n-1} + M_{n-1,n-1}L_{n,n-1}D_n = Y_{n-1} \quad \rightarrow\quad D_{n-1} = \frac{Y_{n-1}}{M_{n-1,n-1}} - L_{n,n-1}D_n$$

$$\vdots$$

$$\text{etc} \tag{73}$$

34

Most of the computational time for this method is expended during the decomposition (Equation 63), because the forward and backward substitutions require very little effort. Note that the decomposition is independent of the loads or the number of separate loading conditions. Therefore, an analysis using multiple loading conditions requires a single decomposition with a forward and backward substitution repeated for each loading case.

Reanalysis Techniques

Repeating the entire finite element analysis for each possible condition is so expensive it severely restricts the amount of damage analysis being conducted. Therefore, the following reanalysis method has been developed to reduce the cost, allowing comprehensive vulnerability analysis to be performed (Ref 5). Assume the original structure is analyzed by the described finite element program, then the equilibrium equation for the structure is Equation 23. When the structure is damaged, the equilibrium equation changes to the following form

$$\underline{K}^* \underline{D}^* = \underline{P} \tag{74}$$

where $\underline{K}^*$ is the actual stiffness matrix and $\underline{D}^*$ is the actual response for the damaged case. The main objective of a reanalysis technique is to build an approximate solution of the modified structure, $\underline{D}^*$, using the information generated during analysis of the original structure, Equation 23 and the known changes. Therefore, the response of the damaged structure can be written in the form

$$\underline{D}^* = \underline{D} + d\underline{D} \tag{75}$$

where the displacement vector $\underset{\sim}{D}$ is the solution of the original undamaged structure, and vector $d\underset{\sim}{D}$ is the true perturbed solution of the damaged structure. The perturbed solution can be estimated by a truncated Taylor series expansion as follows (Ref 5):

$$\underset{\sim}{D} + d\underset{\sim}{D} \simeq \underset{\sim}{D} + \sum_{i=1}^{h} \frac{\partial \underset{\sim}{D}}{\partial g_i} dg_i + \frac{1}{2!} \sum_{i=1}^{h} \sum_{j=1}^{h} \frac{\partial^2 \underset{\sim}{D}}{\partial g_i \partial g_i} dg_i dg_j \tag{76}$$

where g_i is an implicit parameter whose change will affect the stiffness of the ith element. There are h ways in which the stiffness of the structure can be affected. The differential change in response can be written as

$$d\underset{\sim}{D} = \sum_{i=1}^{h} \frac{\partial \underset{\sim}{D}}{\partial g_i} dg_i + \frac{1}{2!} \sum_{i=1}^{h} \sum_{j=1}^{h} \frac{\partial^2 \underset{\sim}{D}}{\partial g_i \partial g_j} dg_i dg_j \tag{77}$$

Multiplying Equation 77 by the original stiffness matrix $\underset{\sim}{K}$ gives

$$\underset{\sim}{K}d\underset{\sim}{D} = \underset{\sim}{K} \sum_{i=1}^{h} \frac{\partial \underset{\sim}{D}}{\partial g_i} dg_i + \frac{\underset{\sim}{K}}{2!} \sum_{i=1}^{h} \sum_{j=1}^{h} \frac{\partial^2 \underset{\sim}{D}}{\partial g_i \partial g_j} dg_i dg_j \tag{78}$$

Since the loads, $\underset{\sim}{P}$, are not dependent on the g_i, differentiating the original *equilibrium* equation (Equation 23) with respect to g_i gives

$$\frac{\partial \underset{\sim}{K}}{\partial g_i} \underset{\sim}{D} = - \underset{\sim}{K} \frac{\partial \underset{\sim}{D}}{\partial g_i} \tag{79}$$

Then differentiating Equation 79 with respect to g_j gives

$$\underset{\sim}{K} \frac{\partial^2 \underset{\sim}{D}}{\partial g_i \partial g_j} = - 2 \frac{\partial \underset{\sim}{K}}{\partial g_j} \frac{\partial \underset{\sim}{D}}{\partial g_i} - \frac{\partial^2 K}{\partial g_i \partial g_j} \underset{\sim}{D} \tag{80}$$

36

Consider the last term in Equation 80, i.e., $\dfrac{\partial^2 \underline{K}}{\partial g_i \partial g_j} \underline{D}$, in relation to

the construction of the stiffness matrix $\underline{K}$, defined by Equation 20.

Examine an arbitrary term from Equation 20

$$\underline{a}_i^T \underline{k}_i \underline{a}_i$$

Since the effects of g_j are limited to the jth element, the ith element

is independent of g_j or

$$\frac{\partial \underline{k}_i}{\partial g_j} = 0 \qquad i \neq j \tag{81}$$

In addition, $\underline{k}_i$ is assumed linear in g_i giving

$$\frac{\partial^2 \underline{k}_i}{\partial g_i \partial g_i} = 0 \tag{82}$$

Therefore, the summation of Equation 20 gives

$$\frac{\partial^2 \underline{K}}{\partial g_i \partial g_j} \underline{D} = 0 \tag{83}$$

Substituting Equations 79, 80 and 83 into Equation 78 gives

$$\underline{K} d\underline{D} = - \sum_{i=1}^{h} \frac{\partial \underline{K}}{\partial g_i} \underline{D} \, dg_i + \sum_{i=1}^{h} \sum_{j=1}^{h} \frac{\partial \underline{K}}{\partial g_j} \frac{\partial \underline{D}}{\partial g_i} d_{gi} d_{gj} \tag{84}$$

Then Equation 84 can be written as

$$\underline{K} d\underline{D} = - d\underline{K}(\underline{D} + d\underline{D}) \tag{85}$$

where

$$dK = \sum_{j=1}^{h} \frac{\partial K}{\partial g_j} d_{gj}$$

and

$$dD = \sum_{i=1}^{h} \frac{\partial D}{\partial g_i} dg_i$$

The iterative algorithm for the perturbed solution can now be written from Equation 85 as

$$KdD^{q+1} = - dK(D + dD^q) \tag{86}$$

where q is the cycle of iteration.

It is very important to note through a comparison of Equation 23 and Equation 86 that no new analysis is required in solving Equation 86. Although the solution of Equation 23 gives the unknown displacement vector D for a known load vector P while in Equation 86 the objective is to solve for the perturbed displacement vector dD^{q+1}, the stiffness matrix K is the same in both equations. Since the stiffness matrix was already decomposed using Equation 63 for the original undamaged structure it is available for the solution of Equation 86, and does not need to be computed in each iteration. Therefore the solution of Equation 86 reduces to the forward and backward substitution steps which are the least expensive of the total solution steps.

Estimation of the Effects of Yielding

In most everyday problems structural loads are designed to fall within the linear range, i.e., the loadings under consideration

generate stresses in each element such that Young's modulus is a con-
stant (See Figure 4). However, with the inclusion of thermal effects,
the proportional limit can be reduced or the addition of thermal
stresses can put the solution outside the linear regime. Therefore the
reanalysis program must be able to handle the effects of material non-
linearities. The most common method for introducing material nonlinear--
ities into the finite element analysis of structures is the piecewise
linear analysis procedure (Ref 15). This procedure uses the superposi-
tion of a series of linear steps. The applied load is divided into a
number of small load steps, and the stress-strain curve is approximated
by a series of straight lines (Figure 5) which are used to calculate the
variation of Young's modulus with stress level. Each load step is
applied sequentially with the Young's modulus in each step determined
from the stress level in each member calculated in the previous step.
The total solution is obtained by adding the solution of each step to
the previous solution, until the full load is reached. This procedure
requires many solutions of Equation 23 in the following form

$$\underset{\sim}{K}^S \Delta \underset{\sim}{D}^S = \Delta \underset{\sim}{P}^S$$

where $\underset{\sim}{K}^S$ is the current stiffness matrix using the appropriate Young's
modulus for the level of stress at step s, $\Delta \underset{\sim}{D}^S$ are the displacements for
step s, and $\Delta \underset{\sim}{P}^S$ is the load increment for step s. Normally a minimum of
6 to 8 steps is required for realistic results. For the case of large
structures computing 6 to 8 solutions is very costly. This cost can be
reduced considerably by a modification of the iterative technique des-
cribed in the previous section. Since the nonlinear effects consist of
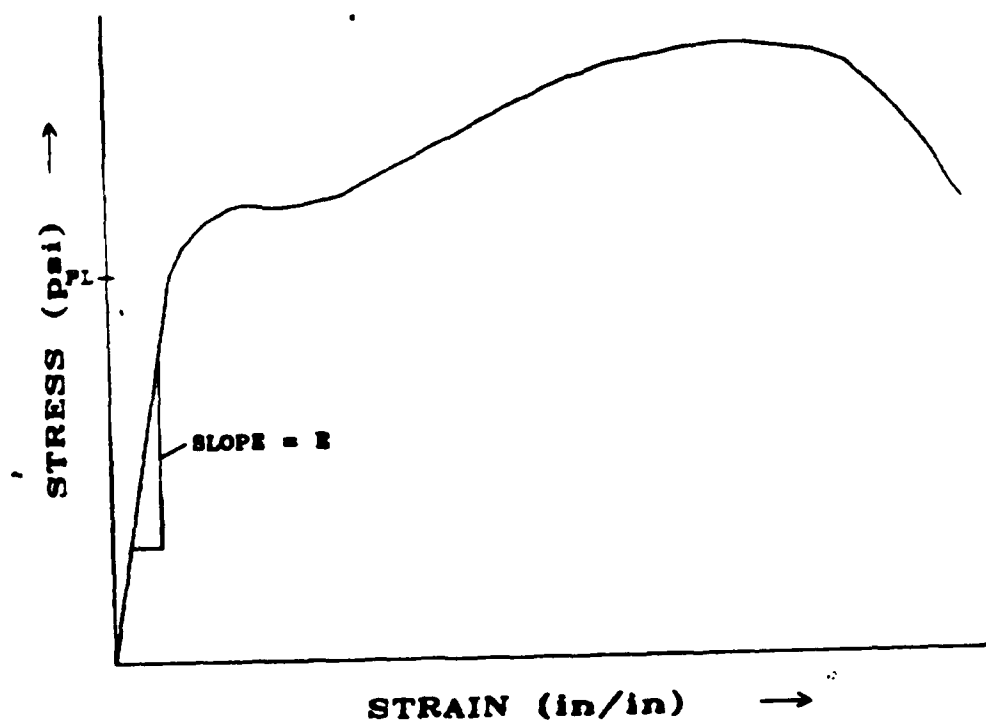Young's modulus changes which were previously included in the definition
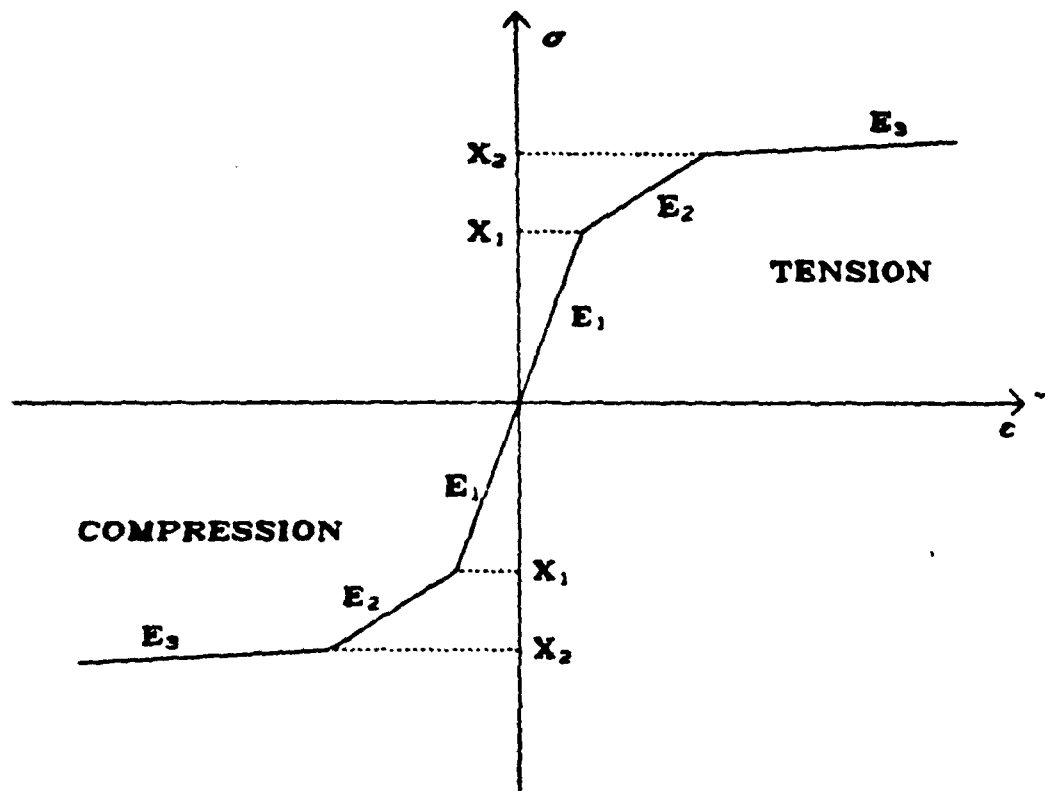
39

Figure 4.   Typical Stress—Strain Curve

Figure 5.   Stress–Strain Curve by Straight Line Approximation

of the stiffness change parameter g_i in Equation 82, the only adjustment
needed to the iterative technique is to determine the amount of load to
include with each change of Young's modulus.

As before, the first step in the procedure is to make a linear
analysis of the structure with the full load using the initial Young's
modulus. The effective stress ratios for each element are calculated
using the modified Von Mises criterion (Ref 16) defined by

$$\theta_i^{(j)} = \sqrt{\left(\frac{\sigma_x}{X_j}\right)_i^2 + \left(\frac{\sigma_y}{Y_j}\right)_i^2 - \left(\frac{\sigma_x\sigma_y}{X_jY_j}\right)_i + \left(\frac{\sigma_{xy}}{Z_j}\right)_i^2}$$

where $\theta_i^{(j)}$ is the effective stress ratio for the ith element at the jth
break of the stress-strain curve, σ_x, σ_y and σ_{xy} are the actual stresses
in the element and X_j, Y_j and Z_j are the respective stresses correspond-
ing to the jth break in the stress-strain diagram (Figure 5).

For simplicity the following derivation will assume a single break
in the stress-strain curve. The elements can then be divided into
elastic and inelastic groups, i.e., those whose stress levels fall with-
in the first and the second straight line segments of the stress-strain
curve, respectively. Elements with $\theta \leq 1$ belong to the elastic group,
while those with $\theta > 1$ belong to the inelastic group. Using the effec-
tive stress ratio, θ, two load factors are defined as

$$\lambda = \frac{1}{\theta_{max}}$$

and

$$\mu = (1 - \lambda)$$

where θ_{max} is the maximum effective stress-ratio of all the elements,

λ is the linear percent of the load or that portion of the stress bounded by the break in the stress-strain curve and μ is the remaining percent. The total applied load is divided into two parts as follows

$$\underline{P} = \lambda\underline{P} + \mu\underline{P}$$

The total response can be divided into corresponding displacement vectors by simple scaling as given by

$$\underline{D}^{\lambda} = \lambda\underline{D}$$

$$\underline{D}^{\mu} = \mu\underline{D}$$

where $\underline{D}^{\lambda}$ is the response up to the break and $\underline{D}^{\mu}$ is the remaining response. Since the initial solution was calculated using the Young's modulus defined by the first segment of the stress-strain curve, $\underline{D}^{\lambda}$ is the valid solution for that portion of the problem. However, Young's modulus changes in the second portion. Therefore the solution for the second segment can be determined by the iterative technique as follows

$$\underline{K}d\underline{D}^{q+1} = - d\underline{K}(\underline{D}^{\mu} + d\underline{D}^{q}) \tag{87}$$

Here $\underline{K}$ is the original linear elastic stiffness matrix and $d\underline{K}$ is the change in the stiffness matrix defined by

$$d\underline{K} = \sum n_i a_i^T k_i$$

where the summation is over those elements exceeding the proportional limit, and $n_i = (E_i^1 - E_i^2)/E_i^1$ where E_i^1 and E_i^2 are the respective Young's moduli for each segment. As described in the previous section this solution requires only forward and backward substitutions repeated for

43

each iteration cycle.

The total response of the structure is given by

$$\underset{\sim}{D}{}^{\star} = \underset{\sim}{D}{}^{\lambda} + \underset{\sim}{D}{}^{\mu} + d\underset{\sim}{D}{}^{q+1} = \underset{\sim}{D} + d\underset{\sim}{D}{}^{q+1}$$

$$\underset{\sim}{\sigma}{}_{i}^{\star} = \underset{\sim}{\sigma}{}_{i}^{\lambda} + \underset{\sim}{\sigma}{}_{i}^{\mu} + d\underset{\sim}{\sigma}{}_{i}^{q+1} = \underset{\sim}{\sigma}{}_{i} + d\underset{\sim}{\sigma}{}_{i}^{q+1}$$

where $d\underset{\sim}{D}{}^{q+1}$ is the displacement vector obtained from Equation 87, and $d\underset{\sim}{\sigma}{}_{i}^{q+1}$ is the stress vector in the ith element due to the displacement vector $d\underset{\sim}{D}{}^{q+1}$. In all these computations it is assumed that Poisson's ratio does not change during yielding.

An extension of this technique to the case of multiple breaks, b, in the stress-strain curve is simply a repetition of the procedure as new breaks are encountered. The load factors for each break are computed by

$$\lambda^{(j)} = \frac{1}{\Theta_{max}^{(j)}}$$

$$\mu^{(j)} = \lambda^{j+1} - \lambda^{j}$$

Using the above definitions the solution for each section can be determined from Equation 87. The total response can be written as

$$\underset{\sim}{D}{}^{\star} = \underset{\sim}{D}{}^{\lambda} + (\underset{\sim}{D}{}^{\mu^{2}} + d\underset{\sim}{D}{}^{\mu^{2}}) + (\underset{\sim}{D}{}^{\mu^{3}} + d\underset{\sim}{D}{}^{\mu^{3}}) + \ldots + (\underset{\sim}{D}{}^{\mu^{b}} + d\underset{\sim}{D}{}^{\mu^{b}})$$

Convergence Criterion

The solution converges if the perturbed solution can be written as

$$dD = \lim_{q \to \infty} dD^q \tag{88}$$

where dD^q is obtained from Equation 86 (Ref 5). To show the convergence criteria for this solution technique, Equation 86 can be written as

$$dD^{q+1} = - K^{-1} dK (D + dD^q) \tag{89}$$

Substituting the iterative results into Equation 89 one obtains

$$dD^{q+1} = [I + \phi + \phi^2 + \phi^3 + \ldots + \phi^q] \phi D \tag{90}$$

where

$$\phi = - K^{-1} dK \tag{91}$$

The superscripts in Equation 90 are exponents denoting powers of the matrix ϕ. However, the exponent on the last term, q, is equal to the number of iteration cycles performed. From Equation 90 the iteration converges only if $[I + \phi + \phi^2 + \ldots + \phi^q]$ converges. Note that the convergence depends on the nature of the matrix ϕ. However, if $\phi^q \to 0$ as $q \to \infty$, the solution converges. This condition exists for small changes in the structural stiffness (Ref 9).

It is important to stress that assurance of convergence is not the sole justification for using this iterative technique. To be useful this technique must be considerably cheaper than direct analysis of the modified model for the damaged structure. The computation time required for this method depends on the number of iteration cycles needed for the

solution, and the rate at which the solution converges depends on the amount of change in the stiffness matrix as shown in Equation 89. A measure of the effectiveness of this procedure could be done by an analysis of the number of calculations performed. However, many variables such as the variable bandwidth of the stiffness matrix, the number of elements damaged, the type of elements damaged and the number of iterations to be performed are either very problem dependent or very hard to predict. Therefore actual run times were used to evaluate the effectiveness of this technique. This produced the estimate that the run time for approximately 30 cycles of iteration is equivalent to the time required for one direct analysis of the damaged structure. Minor damages require 3-5 iteration cycles, medium damage requires 5-15 cycles, while major damage resulting in collapse of the structure requires 15-30 cycles (Ref 5). These results show that for many damage cases the iterative technique will be cost effective.

The criterion for convergence used in most simple iteration schemes is the amount of change of the solution from one iteration to the next. However, in this problem the solution must be in a state of equilibrium requiring

$$\Lambda^q = U^q \tag{92}$$

where Λ^q is the work of the external forces for iteration q given by

$$\Lambda^q = \frac{1}{2} \underline{P} \underline{D}^q \tag{93}$$

and U^q is the internal strain energy of cycle q, defined as

$$U^q = \frac{1}{2} \sum_{i=1}^{n} \int_{V_i} \sigma_i^{q^T} \varepsilon_i^q dV_i \tag{94}$$

From Equation 93 the magnitude of $\Lambda^{q+1} - \Lambda^q$ depends on the magnitude of the loads as well as $D^{q+1} - D^q$. Thus the rate of change of the displacements is not a valid criterion for convergence. However, Equation 92 could be used as a criterion for convergence. Although the calculation of Λ^q is inexpensive requiring only the scalar product of two vectors, the calculation of U^q is very expensive requiring the calculation of the stresses and strains for all the elements. Therefore to reduce the calculations necessary to check for convergence, the work of the external forces is defined as

$$\Lambda^q = \Lambda + d\Lambda^q$$

where Λ is the work of the external forces on the original undamaged structure and $d\Lambda^q = \frac{1}{2} \underline{P} d\underline{D}^q$ is the work of the external forces resulting from the perturbed solution. Then the rate of change in $d\Lambda^q$ can be used as an intermediate criterion for convergence. When it falls within a predefined limit, the strain energy U^q and the work Λ^q can be determined. If the difference between these two quantities is over a prescribed bound, the limit for the rate of change in $d\Lambda^q$ is reduced, and the iteration is continued. Otherwise the solution is considered to have converged.

III. Modeling the Thermal Effects

In order to evaluate the structural damage caused by a laser strik-
ing the structure, a method must be developed to model the thermal
effects of the beam. Although there are many configurations of a laser
beam striking an aircraft structure, which would involve the incidence
of the beam and the curvature of the structure, the scope of this study
will be limited to the basic situation of a continuous stationary laser
beam striking a flat plate at a normal incidence. The beam is consid-
ered axially symmetric so that heat flux occurs only in the axial and
radial directions. This study will examine the effect that the absorbed
flux has on the structure. The effects of the surrounding medium and
the absorptivity of the plate are taken into account by properly adjust-
ing the absorbed flux. The effects of heat loss from the heated plate
have also been ignored, since the additional complexity required to in-
clude realistic radiation or convection loss conditions cannot be justi-
fied by the small impact they would have on the problem (Ref 17).

The thermal effects to be included are the loss of structure due to
melting, the induced thermal stresses resulting from thermal expansion,
and the change in material properties due to temperature dependence.
Although other effects could be included, these represent the major
damage mechanisms from a structural point of view.

Heat Conduction Problem

The purpose of the heat conduction problem is to determine the tem-
perature distribution from which the amount of melting, the thermal
stress, and the change in material properties can be determined. Tem-
perature distributions are solutions to the differential equation for

48

AFIT/GAE/AA/83M-1

heat transfer.

$$C_p \rho \frac{\partial T}{\partial \tau} = \frac{\partial}{\partial x}\left[\frac{k \partial T}{\partial x}\right] + \frac{\partial}{\partial y}\left[\frac{k \partial T}{\partial y}\right] + \frac{\partial}{\partial z}\left[\frac{k \partial T}{\partial z}\right] + Q$$

where

C_p = specific heat (Btu/lbm °F)

ρ = density (lbm/in^3)

T = temperature (°F)

k = thermal conductivity (Btu/Sec in °F)

τ = time (sec)

Q = rate of energy gain due to laser flux absorbed (Btu/in^2 sec)

x,y,z = orthogonal directions

Consider the flat plate to be a cylindrical disk and the prescribed flux to vary only in the radial direction. Then no heat transfer occurs in the circumferential direction, and the problem reduces to two-dimensions in a cylindrical coordinate system. Exact solutions have been found for this problem for constant properties and temperatures below melting. However, for problems with a sufficiently large flux to cause temperatures to reach the melting point, available exact solutions are limited to the case of one dimensional problems subjected to a uniform flux. Therefore, a numerical solution must be used.

The solution could be found using a finite element analysis similar to the technique described in Section II. But, since the problem is time dependent, the solution would require a complete analysis at each time step. Similarly, the use of a traditional finite difference approach also requires a matrix inversion at each time increment.

Therefore, the numerical approach used in this study is a modification of an explicit technique that was initially reported by Dusinbeere (Ref 18). This technique is based on dividing the disk into finite cells and performing a heat balance on each. The advantage to this approach is that it requires less computer storage and run time than either of the traditional approaches and yields comparable results (Ref 1).

Numerical Solution

The first step in this procedure is to divide the disk into a number of finite cells. The thickness, h, of the disk is divided into a number, N_C, of layers, and similarly the radius, r, is divided into N_R, sections. Since the structural model in this study was generated with elements of a single material, each cell is taken to have the same properties. For simplicity, the following development assumes that all divisions are equal through the thickness and that each of the radial divisions are of equal length, however, only minor changes would be required to allow for unequal divisions. Thus the disk is modeled as $N_C \times N_R$ cells (Figure 6.a). Each cell is then referenced as a two dimensional array, where the first index refers to the thickness layer and the second refers to the radial division (Figure 6.b). By using this indexing scheme all properties associated with cell i,j can be referenced in the same manner.

Consider a typical cell shown in Figure 7. Cell i,j is surrounded by four other finite cells, and heat conduction is the only form of heat transfer. Using Fourier's law of heat conduction

$$Q = - kA \frac{\partial T}{\partial x}$$
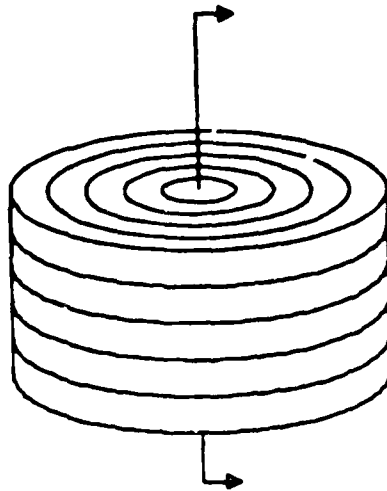
(a) Discretizing the Area of Thermal Influence
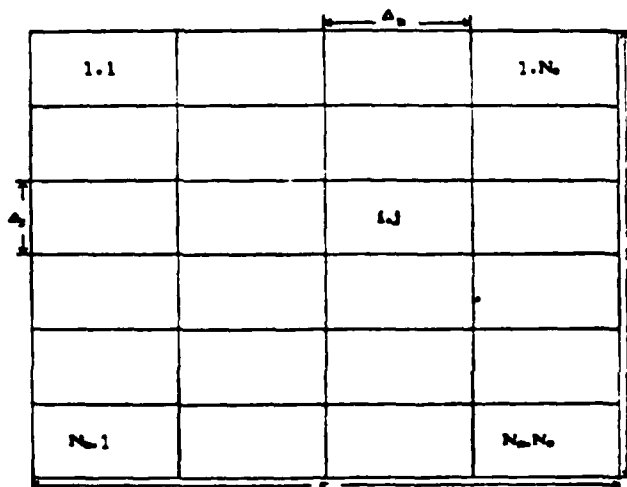
(b) Indexing Scheme for the Thermal Cells

Figure 6. Division of Disk into Finite Cells
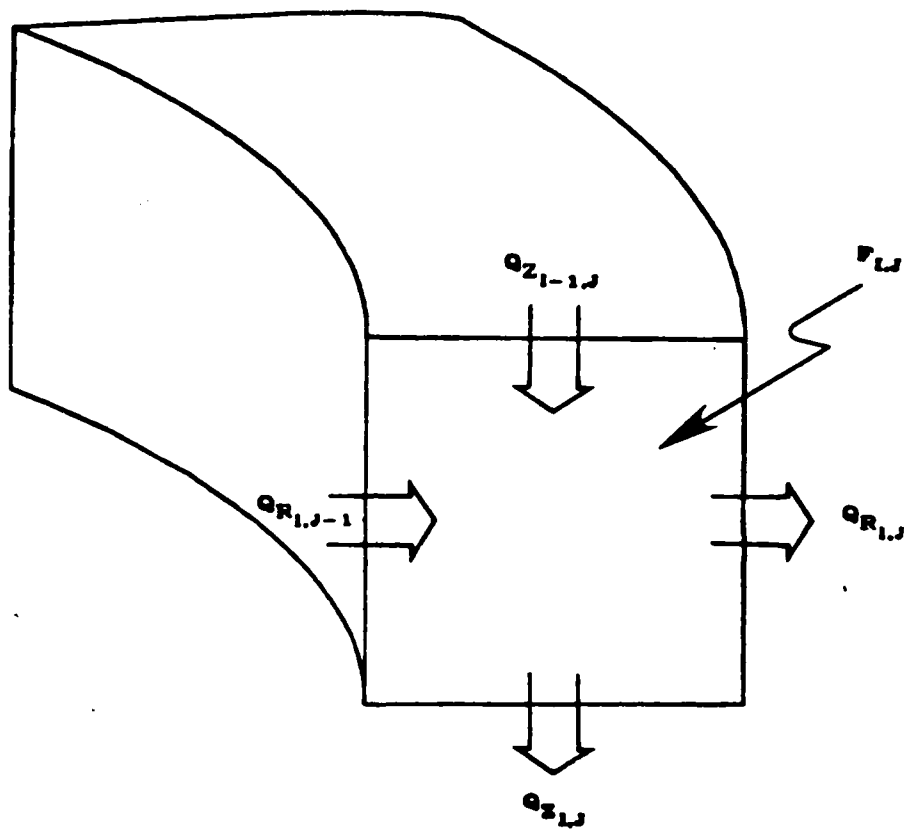
Figure 7.   Heat Balance on Each Cell

where A is the area normal to the direction of the heat flow and x is the variable length between the points of interest, the approximation for the heat flow conducted out of cell i,j can be given as

$$Q_{Ri,j} = k_{Ri,j} A_{Ri,j} \frac{T_{i,j} - T_{i,j+1}}{\Delta_R}$$

and

$$Q_{Zi,j} = k_{Zi,j} A_{Zi,j} \frac{T_{i,j} - T_{i+1,j}}{\Delta_Z}$$

Here Q is the heat conducted, Δ the length the heat travels, and the subscripts R and Z denote the radial and axial directions respectively.

To perform a heat balance on each element, it is necessary to consider the location of the element with respect to the entire disk. If an element is located on the surface of the disk, it is possible that energy, $F_{i,j}$, could be added by the absorption of external flux due to the laser, and there would not be convected energy incoming from the thickness direction since there are no cells above it, i.e., from a cell of lower index i. For the center cells, incoming conduction in the radial direction is zero, since they are solid disks. In addition, the bottom cells and outer edge cells have no outgoing convected energy in the thickness and radial directions, respectively, due to the imposed insulated boundary conditions. These are accounted for by setting to zero the appropriate Q. Considering each cell to have flux values and convection terms on all four sides, and combining the external flux term with the incoming convected energy terms and subtracting the outgoing energy terms, the general expression for the heat balance of

53

cell i,j is given by

$$\Delta Q_{i,j} = F_{i,j} + Q_{Ri,j} + Q_{Zi,j} - Q_{Ri,j} - Q_{Zi,j}$$

where $\Delta Q_{i,j}$ is the amount of energy remaining to cause a change in the temperature of cell i,j.

Providing the melting temperature has not been reached, the temperature rise in cell i,j during a time increment $\Delta\tau$ can be written as

$$\Delta T_{i,j} = \frac{\Delta Q_{i,j}\Delta\tau}{C_{pi,j}M_{i,j}}$$

where $M_{i,j}$ is the mass of cell i,j.

Melt Calculations

In some later time increment, $\Delta\tau$, the temperature will reach the melting temperature. When the melting point is reached, the cell has not actually melted, and more energy must be added to bring about the complete phase transformation of all the mass in the cell. Thus, the total energy required to melt cell i,j after it has reached the melting temperature is given by

$$\gamma^{o}_{i,j} = \Gamma_{i,j}M_{i,j}$$

where $\Gamma_{i,j}$ is the heat of fusion. To model this phenomena an energy bank is established for each cell with the appropriate $\gamma^{o}_{i,j}$ value. Then, once the cell i,j reaches the melting temperature, $\Delta\tau\Delta Q_{ij}$ is subtracted from $\gamma^{o}_{i,j}$, and the temperature of the cell is held at melting. At ℓ time increments after cell i,j reaches melting temperature

$$\gamma_{i,j} = \gamma^{o}_{i,j} - \sum_{\beta=1}^{\ell} \Delta Q^{(\beta)}_{i,j}\Delta\tau^{(\beta)}$$

54

and the entire cell is presumed to have melted in the time increment
when $\gamma_{i,j} \to 0$.

Since the melted material will add little or no stiffness to the
structure, the melt is considered to be instantaneously removed. There-
fore, the conductivities of that element are set to zero, and any
external flux received is transferred to the cell immediately below,
i.e., *from cell i,j to cell i+1,j.*

Laser Flux Profile

The incident laser flux is assumed to be circular with either a
Gaussian or uniform profile. Neither of these approximations represents
the exact spatial profile, because experience has shown that in reality
hot spots can occur (Ref 19:13). However, the Gaussian profile is con-
sidered, in general, to be a suitable approximation for this type of
parametric study, because of the random nature of the intensity, size,
and location of such hot spots.

If the Gaussian profile is used, the incident energy absorbed by a
cell i,j on the surface is determined by

$$F_{i,j} = F_o A_{Zi,j} e^{(-.5R^2/\sigma^2)}$$

where F_o is the peak absorbed intensity, R is the distance from the cen-
ter of the beam to the center of cell i,j having an area $A_{Zi,j}$, and 2σ
is the radius of the laser beam. The assumed Gaussian beam is actually
of infinite radius, but by defining the beam radius in this manner 86.5%
of the total energy absorbed by the plate is within this radius. $F_{i,j}$
is taken to be zero for $R \to 2\sigma$, thus, the remaining 13.5% of the energy
is neglected.

55

When the uniform profile is selected, the incident energy absorbed is given by

$$F_{i,j} = F_o A Z_{i,j}$$

for $R \leq 2\sigma$ and $F_{i,j} = 0$ for $R \to 2\sigma$.

Results of the Temperature Distribution

The output of the computer program is the response of a structure incurring a laser strike. Although the temperature distribution plays an important part in the final solution, it is not possible to observe only the behavior of the temperature solution once it has been integrated with the structures program. Therefore this section deals with the accuracy of the temperature solutions and discusses the effects that some structural configurations could have on the solution.

To measure the accuracy of the technique, comparisons between the temperature fields predicted by the numerical technique and exact solutions or other approximate solutions were made by Torvik (Ref 1). To ensure the accuracy of the program developed for this study, a comparison was made for the one dimensional heating of an semi-infinite solid. The exact solution, valid to the onset of melting, is given by (Ref 20)

$$T - T_o = \frac{2F_o(\alpha\tau)^{1/2}}{k} \; \text{ierfc}\left\{\frac{x}{2(\alpha\tau)^{1/2}}\right\} \tag{88}$$

where α is the diffusivity, $k/\rho C_p$, and ierfc denotes the first integral of the complementary error function. The front surface temperature is given by

$$T - T_o = \frac{2F_o}{k} \left[\frac{\alpha\tau}{\pi} \right]^{1/2} \tag{89}$$

The comparison was made using the properties of Al_2O_3. This material was chosen as it is a poorer conductor than metals, producing higher thermal gradients and a more stringent test of the numerical process. The properties are:

$\rho = 3.8$ gm/cm^3

$k = 0.104$ joule/(cm sec °c)

$C_p = 0.885$ joule/(gm °c)

$T_{melt} = 2313°K$

$F = 4000$ joules/(cm^2 sec)

$T_o = 300°K$

The temperature profiles, determined using Equations 88 and 89, are plotted at 0.02, 0.04 and 0.06 seconds in Figure 8 as solid lines. The temperature distribution at the mid-points of each cell, determined by the numerical procedure described in the preceeding section using a layer thickness of 0.015 cm and a time step of 0.001 sec, is shown by the asterisks in Figure 8. As can be seen, the results of the exact and numerical solutions are indistinguishable.

In addition to using the numerical solution to calculate known solutions to verify the accuracy of the program, the heat transfer program was used to observe the effects of an internal structure. Relating the temperature distribution to an external surface that can be approximated by a flat plate is a fairly simple procedure involving the calculation of the radial distance a given point from the beam center and
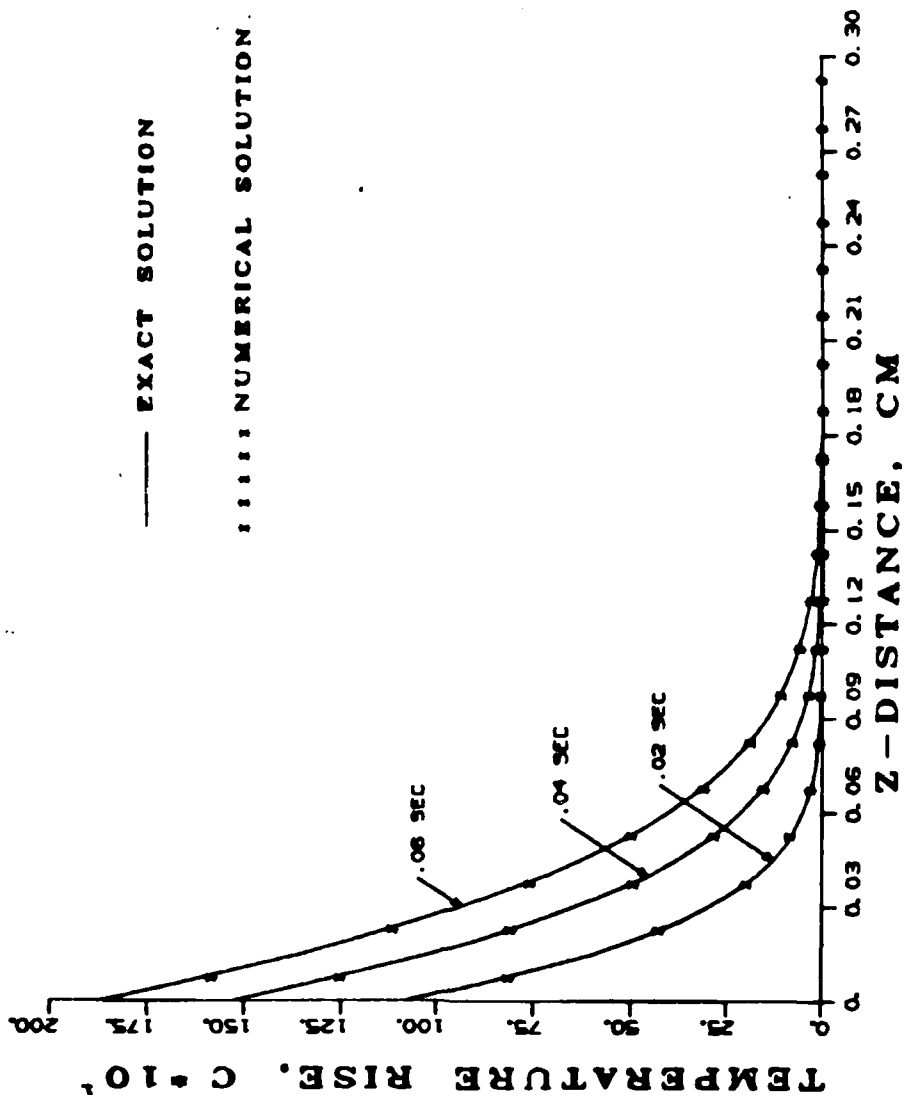
Figure 8. Temperature Distribution for a Semi-infinite Solid

applying the temperature calculated at that distance. However, application to a realistic wing structure involves calculating the effects of ribs and spars and the temperature distributions within them. The addition of structure below the skin will act as a heat sink and could result in a much cooler temperature distribution on the skin. To estimate the effect of inner structure on the temperature distribution, a "worst case" was examined. The "worst case" involved placing an internal structure directly under the beam spot. The resulting temperature distribution was plotted against the temperature distribution calculated for the flat plate. To observe possible effects on the melting mechanism, laser application times of 0.1 and 1.0 sec were used, giving one case with minor surface melting and one case with melt completely through the skin.

For both endurance times the inclusion of internal structure resulted in only slightly lower temperatures within the beam spot. The influence away from the beam diminished with distance (See Figure 9). In addition, the area of the plate removed by melting is not affected. Therefore this study will consider the effects of any internal structure to have no effect on the temperature distribution. This results in a conservative approximation of the damage incurred, due to the slightly hotter temperature solution.
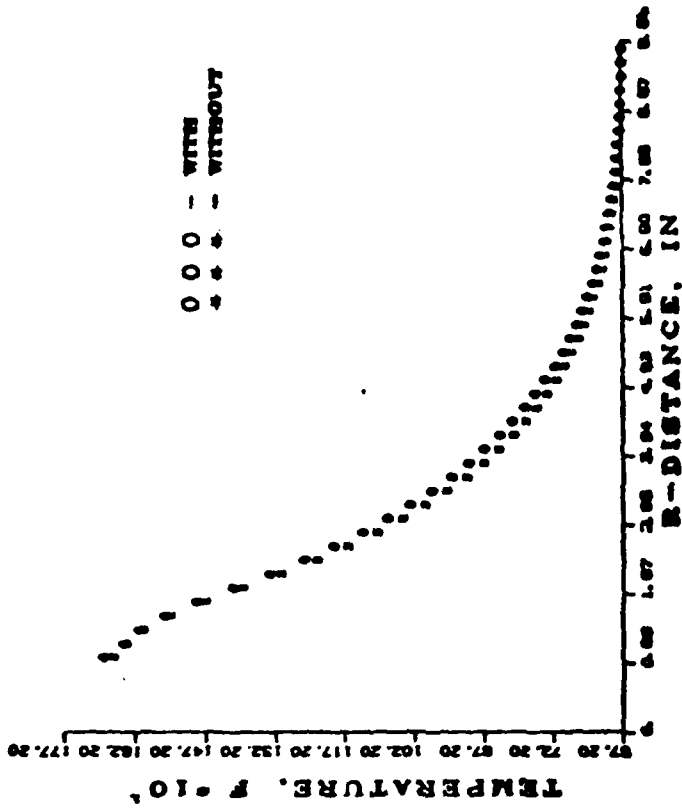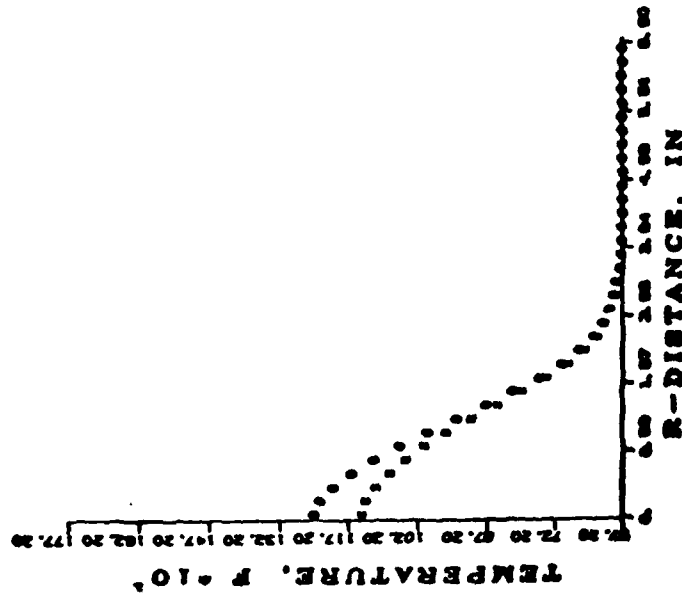
Figure 9. Effect of Internal Structure on the Temperature Distribution

IV Modeling the Damage

Once the heat conduction problem has been solved, the damage incurred by the structure must be modeled. The types of damage to be considered are: loss of structure due to melt, addition of thermal stresses resulting from thermal expansion, and dependence of Young's modulus on temperature.

Damage Due to Material Loss

The damage due to material loss is defined as the loss of stiffness that a finite element incurs when some of its material is removed through melt. In order to model this phenomenon, a parametric study was conducted by modeling a flat plate in a state of tension with holes of varying diameters and depths. The plate and the hole were considered to be symmetric about both the x and y axis. Symmetric boundary conditions reduced the problem to a quarter section of the plate (Figure 10). The symmetric boundary conditions used restricted those points lying on the y-axis from motion in the x direction and those points on the x-axis from motion in the y direction. The symmetry reduction was also considered when the loads were calculated. To simulate a uniform load across the entire edge, the magnitude of the loads at each corner must be halved, because the mirror image symmetric section would also have a node at that point with a equal load.

When the laser beam spot is considered to be round, the material loss will appear as a circular hole partially or entirely through the thickness. Although most of the cases studied consisted of circular holes, non-circular holes were also considered. In an actual structure, non-normal incidence or beam jitter along a preferred axis could produce
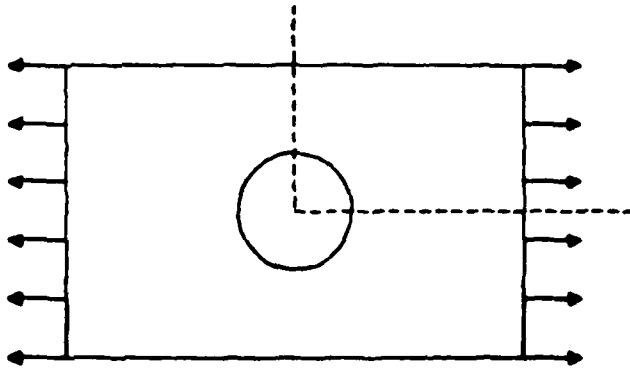
Figure 10.   Flat Plate

a non-circular beam. The resulting damage would then be somewhat oval. Therefore, oval holes through the entire thickness with the major axis transverse to the load were also considered so that the stiffness loss could be compared with that for circular holes.

The stiffness for the damaged plate was calculated as a percent of the stiffness for the undamaged plate by dividing the average edge displacement of the complete plate by the average edge displacement of the damaged plate. The results are shown in Figure 11, where the cases modeling circular holes are represented by solid lines. The cases calculated for oval holes through the entire thickness are shown as asterisks. This data reflects the effect of an elliptical versus a circular shaped hole on the plate and shows the stiffness of plates with oval holes to be greater than those with circular ones. Thus using the circular hole values gives a conservative estimate.

The shape of the sides of the hole must also be considered, because the hole is not in reality a cylinder perpendicular to the plane of the plate. Such an assumption neglects a wedge of material at the lower edge of the hole. However, because of the high temperature, the material in the wedge will not add significantly to the stiffness of the plate and can be neglected. Since the program uses the total energy, $Y_{i,j}$, required to melt cell i,j to determine the time at which cell i,j melts, the percentage of melting for the cell can also be determined from $Y_{i,j}$. The program searches the $Y_{i,j}$ looking for non-zero values to determine the amount of material melted and the dimensions of the hole created. The radial dimension of the melted area is taken to be determined solely by the top layer and the depth of the hole by the center division. Each $Y_{1,j}$ is tested, starting from the center $Y_{1,1}$,
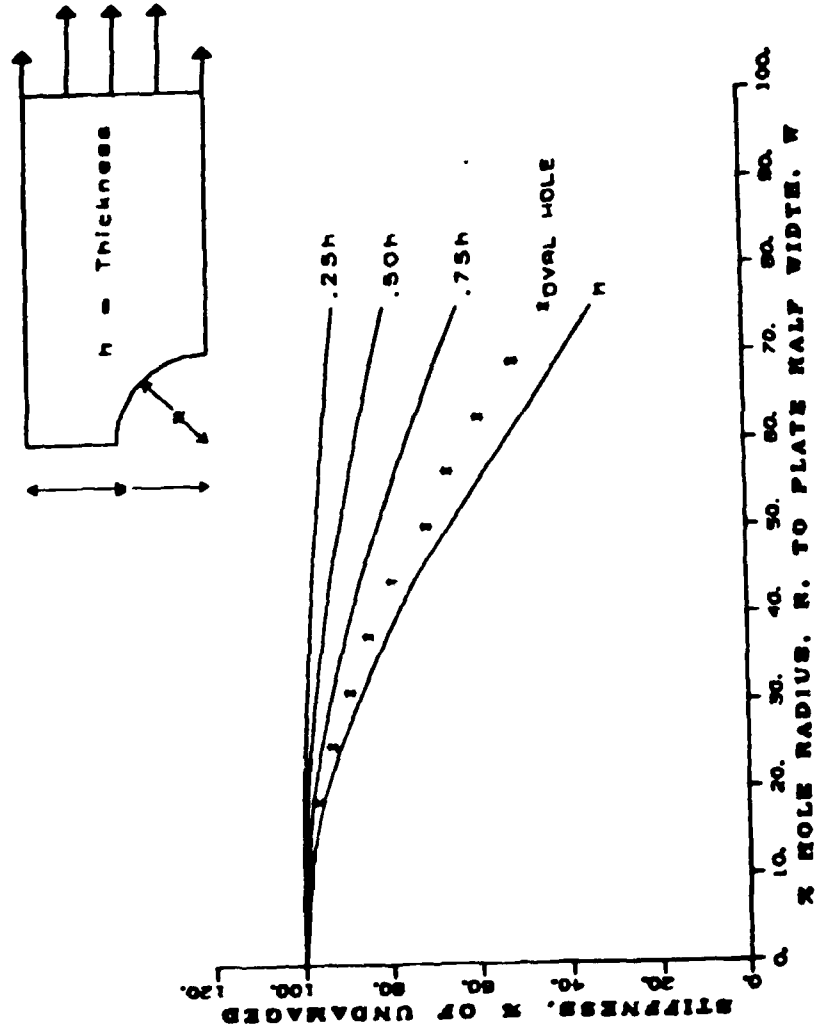
63

Figure 11. Effect of Material Loss

until a value greater than zero is found in γ_{1,N_M}. The radius of the hole is then determined by $RM = N_{MR}\Delta_R$, where N_{MR} is the index of the first non-zero term radially and Δ_R is the length of the radial division. Similarly each $\gamma_{i,1}$ is searched through the thickness giving $TM = N_{MZ}\Delta_Z$, where N_{MZ} is the index of the first non-zero term through the thickness and Δ_Z is the thickness of each layer. The stiffness loss is then determined from the hole's radial and thickness dimensions by interpolating from the data for circular holes presented in Figure 11.

Addition of Thermal Loads

With the heating of elements due to the laser strike, thermal expansion occurs and generates thermal stresses. With the addition of the thermal load, Equation 5 becomes

$$U_i = \int_{V_i} \left(\frac{1}{2} \underset{\sim}{\sigma}_i^T \underset{\sim}{\varepsilon}_i - \underset{\sim}{\sigma}_i^T \underset{\sim}{\varepsilon}_i^0 \right) dV \tag{90}$$

where $\underset{\sim}{\varepsilon}_i^0$ is the thermal strain produced by heating the ith element. $\underset{\sim}{\varepsilon}_i^0$ is given by

$$\underset{\sim}{\varepsilon}_i^0 = \underset{\sim}{\alpha}_i \Delta T_i$$

where $\underset{\sim}{\alpha}_i$ is the vector of coefficients of thermal expansion and ΔT_i is the change in temperature.

The first term in Equation 90 will follow the development presented in Section II. Substituting Equations 6, 8 and 9 into the second term of Equation 90 gives

$$- \int_{V_i} \underset{\sim}{u}_i^T \underset{\sim}{N}_i^T \underset{\sim}{B}_i^T \underset{\sim}{E}_i \underset{\sim}{\varepsilon}_i^0 dV \tag{a}$$

65

Because all elements included in this program are isentropic plane stress elements, the thermal strain vector is given by

$$\varepsilon_i^0 = \alpha_i \Delta T_i \begin{bmatrix} 1 \\ 1 \\ 0 \end{bmatrix} \tag{91}$$

Multiplying (a) by the material property matrix $\underline{E}_i$ gives

$$\underline{E}_i \varepsilon_i^0 = \frac{E_i \alpha_i \Delta T_i}{(1 - \nu_i)} \begin{bmatrix} 1 \\ 1 \\ 0 \end{bmatrix} \tag{92}$$

Since Equation 92 is independent of volume and since all elements in this program were constructed using a linear relationship between the internal and nodal displacements, $\underline{N}_i^T \underline{B}_i^T$ is also independent of volume. Therefore (a) can be written as

$$- \underline{u}_i^T \underline{N}_i^T \underline{B}_i^T \frac{E_i \alpha_i \Delta T_i}{(1 - \nu_i)} \begin{bmatrix} 1 \\ 1 \\ 0 \end{bmatrix} \int_{V_i} dV$$

or

$$- \underline{u}_i^T \underline{N}_i^T \underline{B}_i^T \frac{E_i \alpha_i \Delta T_i}{(1 - \nu_i)} \begin{bmatrix} 1 \\ 1 \\ 0 \end{bmatrix} V_i \tag{b}$$

If

$$\underline{\psi}_i = \underline{N}_i^T \underline{B}_i^T \frac{E_i \alpha_i \Delta T_i}{(1 - \nu_i)} \begin{bmatrix} 1 \\ 1 \\ 0 \end{bmatrix} V_i \tag{93}$$

66

then (b) can be written as

$$- \underline{u}_i^T \underline{\psi}_i \tag{c}$$

With this term Equation 17 gives the following form for the total
potential energy when thermal loads are included

$$\Pi_p = \sum_{i=1}^{n} \left(\frac{1}{2} \underline{u}_i^T \underline{k}_i \underline{u}_i - \underline{u}_i^T \underline{p}_i - \underline{u}_i^T \underline{\psi}_i \right) \tag{94}$$

Substituting the transformation matrix defined in Equation 18 and
letting

$$\underline{\psi} = \sum_{i=1}^{n} a_i^T \underline{\psi}_i$$

the total potential energy becomes

$$\Pi_p = \frac{1}{2} \underline{D}^T \underline{K} \underline{D} - \underline{D}^T \underline{P} - \underline{D}^T \underline{\psi}$$

Taking the first variation with respect to the displacement gives

$$\delta \Pi_p = \delta D^T (\underline{K} \underline{D} - \underline{P} - \underline{\psi})$$

and when the stationary requirement is met the equilibrium equation
becomes

$$\underline{K} \underline{D} - \underline{P} - \underline{\psi} = 0 \tag{95}$$

Combining the nodal forces and the thermal loads as

$$p^* = P + \Psi \tag{96}$$

and substituting into Equation 95 gives

$$KD - p^* = 0 \tag{97}$$

which is exactly the same form as Equation 23. Therefore, by using Equation 94 to calculate the thermal loads and then combining the two load sets, all the equations for the reanalysis technique remain the same and can be used with no modification. It is important to note that the original solution upon which the iterative technique is based must include the affects of the thermal loads.

Temperature Dependence of Young's Modulus

Although the major loss of stiffness to an element would be due to a loss of material caused by melting, the effect on the entire structure would not be significant unless the melt occurred on a major load carrying member. However, due to the high conductivity of metals, a temperature rise can occur over a large section of the structure. This can reduce the magnitude of Young's modulus in a number of elements and result in a major stiffness change for the entire structure. Therefore, changes in Young's modulus can be the major damage mechanism for the structure as a whole.

To apply the temperature dependence affect to this damage program, a table of Young's modulus vs temperature was developed. For the sample problems in this study the Young's modulus vs temperature curve for T2014 aluminium from Mil Handbook 5, Figure 12, was approximated in tabular form. The temperature for each node was calculated from the
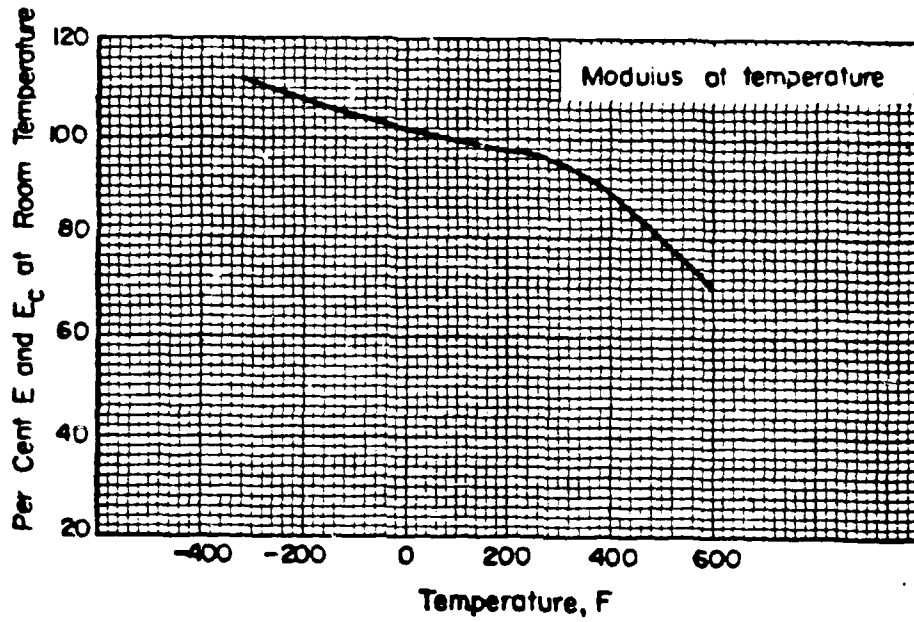
Figure 12.   Young's Modulus Dependence on Temperature

temperature solution, and the elemental temrerature was determined as an average of the nodal temperatures. Using that calculated temperature, an interpolation of the table resulted in the new Young's modulus, E_i', for the element.

The reduction factor to be used in the iterat,ve technique is given as

$$n_i = \frac{E_i - E_i'}{E_i}$$

V Results

The laser damage program developed in the present study was applied to two different structures. These structures are of two different levels of complexity, one being a simple two-dimensional plate and the other a much more refined three-dimensional wing structure. These problems demonstrate the ability of the program to be used for a smaller localized analysis as well as for a large aircraft structure. A complete description of the two structures and the reanalysis results are described in this Section.

Flat Plate

The first structure was a flat plate clamped on one edge, subjected to a uniform tensile loading, and modeled with both triangular membranes (See Figure 13) and quadrilateral membranes (See Figure 14). The material of the structure was assumed to be aluminum with a Young's modulus of $E = 10.0 \times 10^6$ psi and a density of $\rho = 0.1$ lbf/in^3. Six subcases were defined by varying the number and location of elements exposed to the laser strike. Table 1 lists the various cases considered for this structure. The laser size and strength were varied to produce different damage levels for each case.

The overall size of the plate was 12.0 in x 8.0 in x .1 in, and the elements were uniform in size with an area of 2.0 in^2 and 4.0 in^2 for the triangular membranes and the quadrilateral membranes, respectively. This structure was selected because of its simplicity and its size. Since it is a two-dimensional model, the damage effects are easier to understand. Because the plate is small and the conductivity of aluminum is high, the laser strike affected the temperature of all the elements.

71
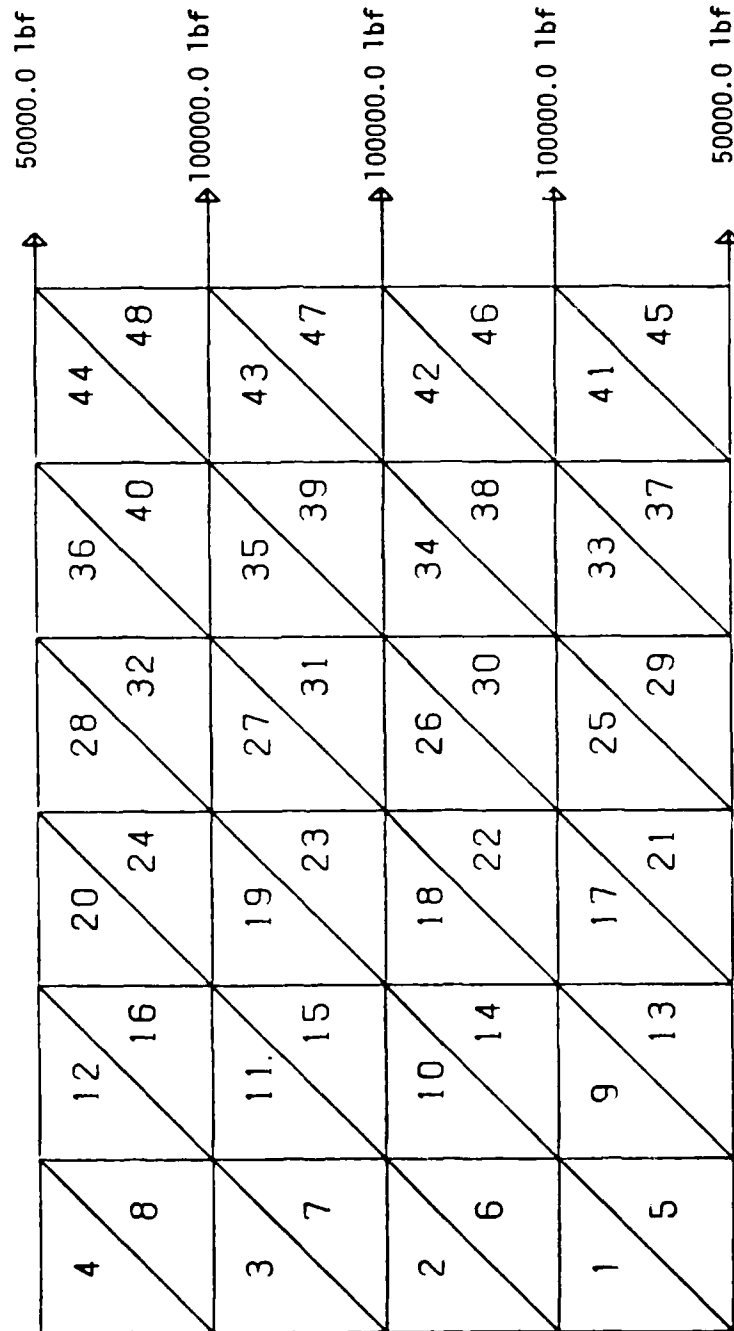
Figure 13. Flat Plate with Triangular Membranes
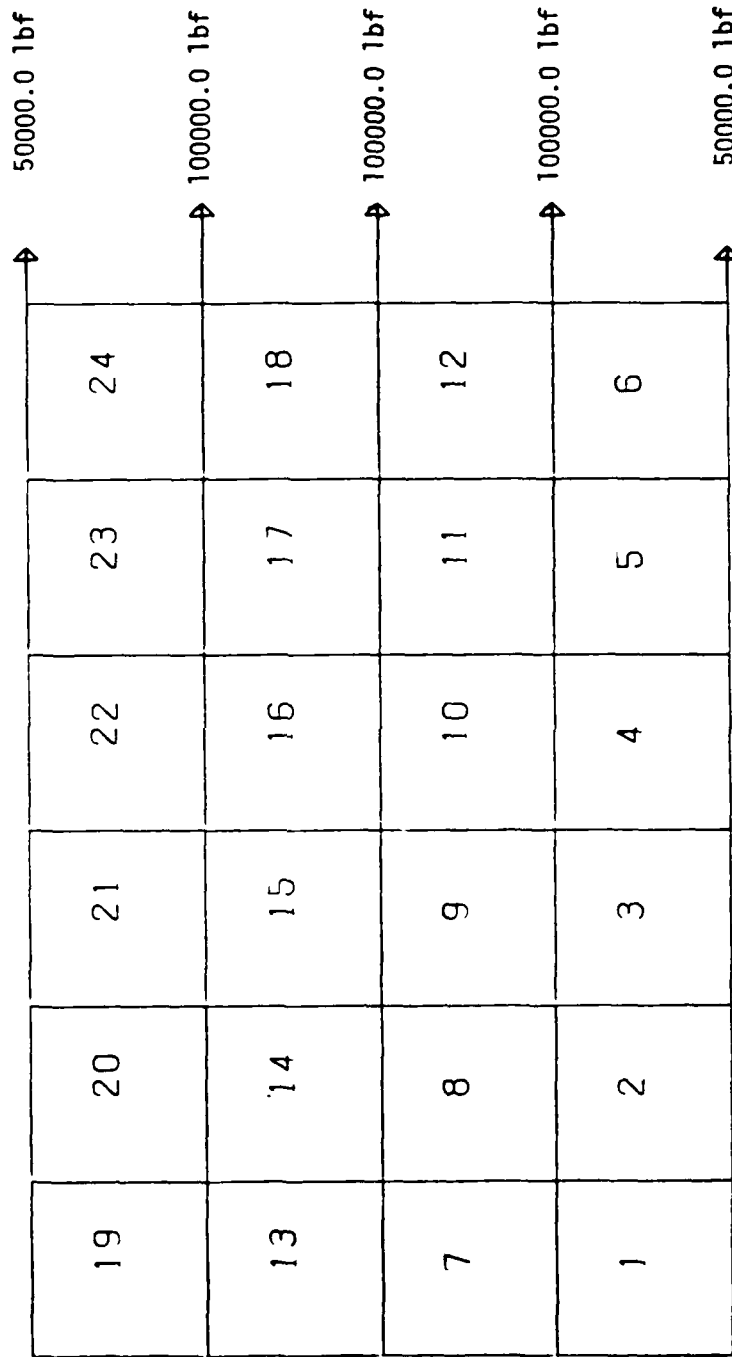
Figure 14. Flat Plate Modeled with Quadrilateral Membranes

Table 1 Description of Flat Plate Cases

Cases	Modeling Element	Elements Struck	F_o (Btu/in^2)	σ (in)	Strike Endurance (sec)
1	Triangular	18	35	.5	.89
2	Triangular	18	25	1.18	.43
3	Triangular	17,24 18,19,22,23	35 25	.5 1.18	.63 .63
4	Quadrilateral	9	35	.5	.63
5	Quadrilateral	9	25	1.18	.43
6	Quadrilateral	3,21 9,15	35 25	.5 1.18	.63 .43

74

These attributes define a model that is easy to verify and will show an entire structure changing rather than the effects of modifying a localized area. As a result, the model is a "worst case" example.

In order to provide a baseline to compare the damage cases, the solution to the original undamaged case was used. The maximum displacement was 0.60 in for both models, and the computer time required was 309 and 331 10-millisecond tics for the triangular membrane model and the quadrilateral membrane model, respectively. The resulting deformed shapes are shown in Figures 15 and 16.

Since the temperature of all the elements changed, thermal loads were generated for all the nodes. Some of these loads were quite large. For example, the maximum magnitude of the nodal loads generated from the thermal effects in Case 1 was 13,880.33 lbf. With such large loads the panels can buckle. However, buckling considerations are not included in this study.

The results for the flat plate cases are summarized in Table 2. In order to visualize the damage effects, the deformed shapes for these cases are shown in Figures 17 through 22. The plots shown in these figures represent both reanalysis and NASTRAN results. The deformed shapes show the expected responses. The figures show the deformed shape skewed to one side representing some in-plane bending. Since the beam does not strike on the center line of the plate, the side of the plate receiving the strike is hotter and incurs more damage. Thus, deformation on the side of the laser strike is greater, resulting in the skewed appearance of the damaged plate (Figures 17-22).

In the cases where the damage appeared minor, i.e., the change in the maximum displacement from the undamaged case was small, the reanalysis technique does not seem to be as efficient as in the case

75
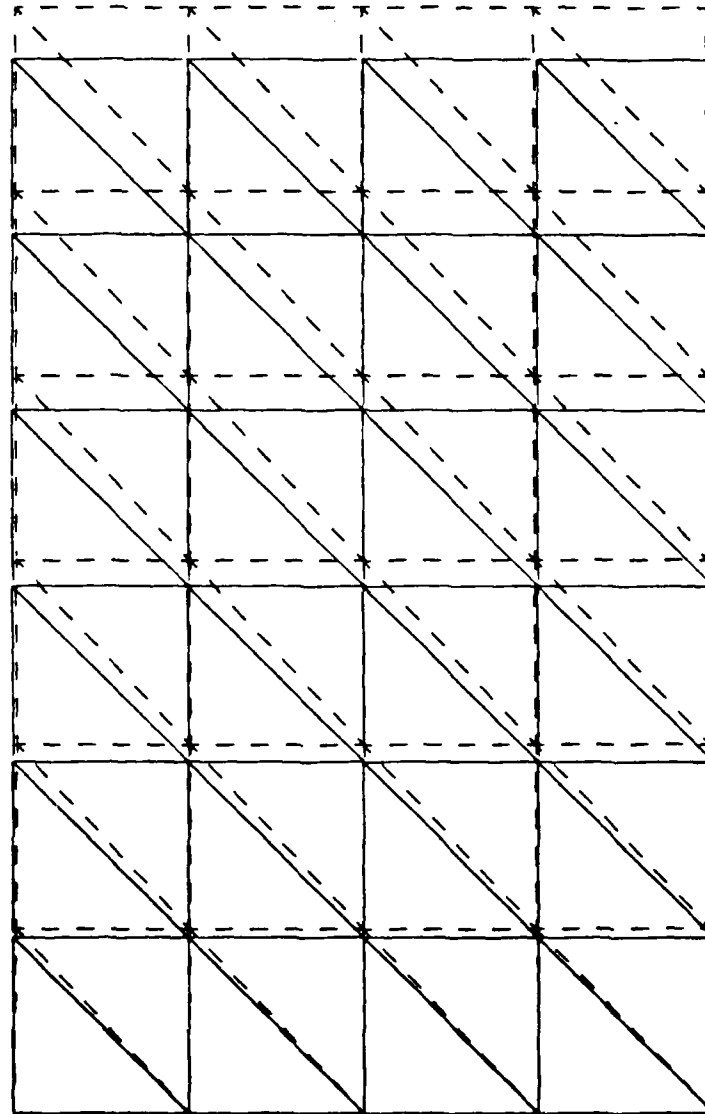
—— Undeformed Shape

---- Deformed Shape

Figure 15. Deformed Shape Undamaged Flat
Plate – Triangular Membranes
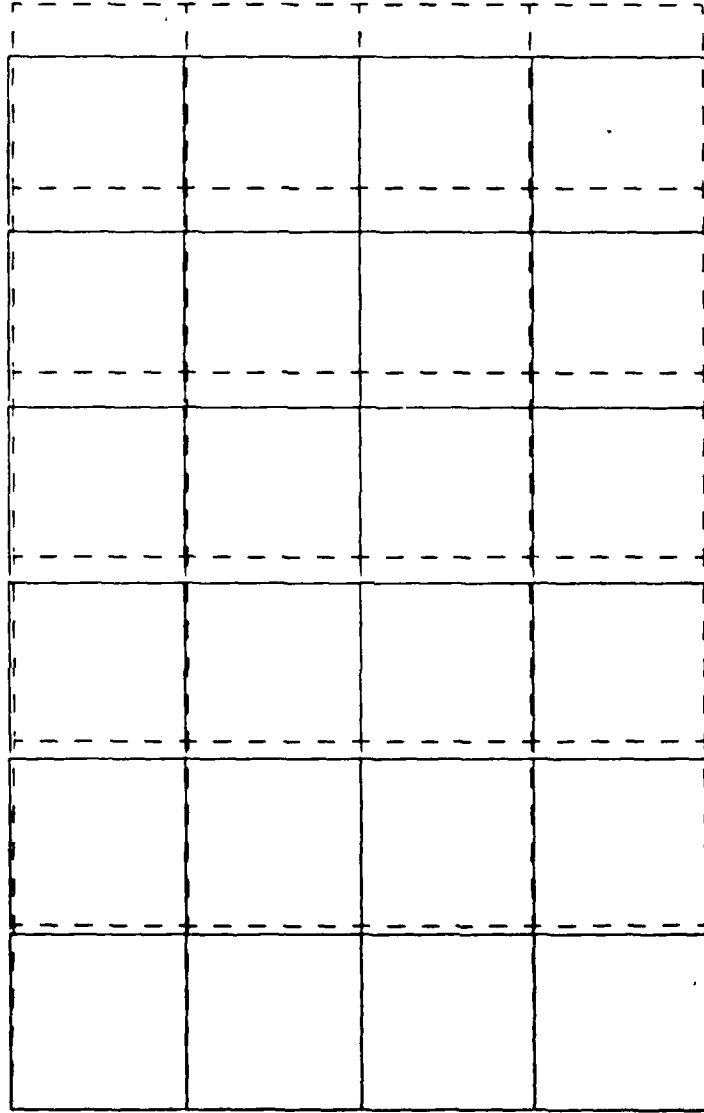
—Undeformed Shape

----Deformed Shape

Figure 18. Deformed Shape Undamaged Flat Plate – Quadrilateral Membranes
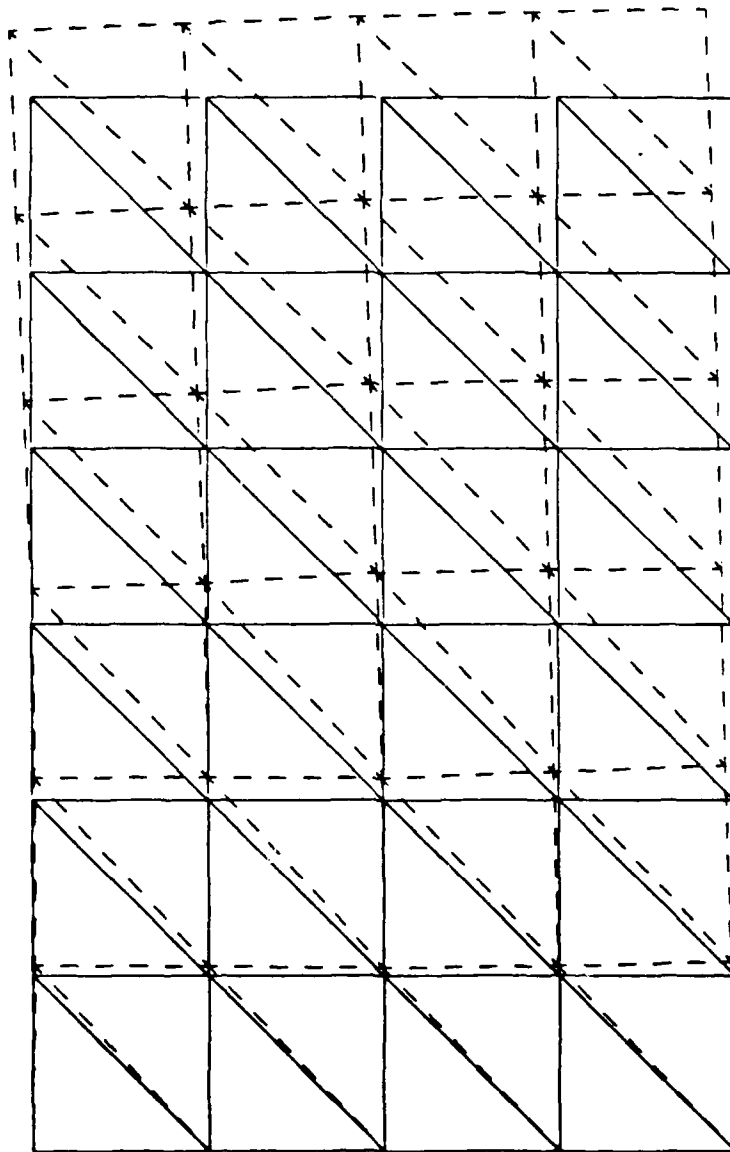
Table 2 Flat Plate Results

Case	Reanalysis Max Disp (in)	NASTRAN Max Disp (in)	% Diff	Iter Time % Undamaged Case	Cycles	Damage Range
1	.7183	.7129	.75	22.98	3	Minor
2	1.0145	1.0132	.13	54.37	10	Medium
3	2.6297	2.6215	.31	462.78	100	Major
4	.6862	.6796	.97	14.50	3	Minor
5	1.1351	1.1347	.03	52.54	14	Medium
6	3.0988	3.0951	.12	213.56	100	Major

78
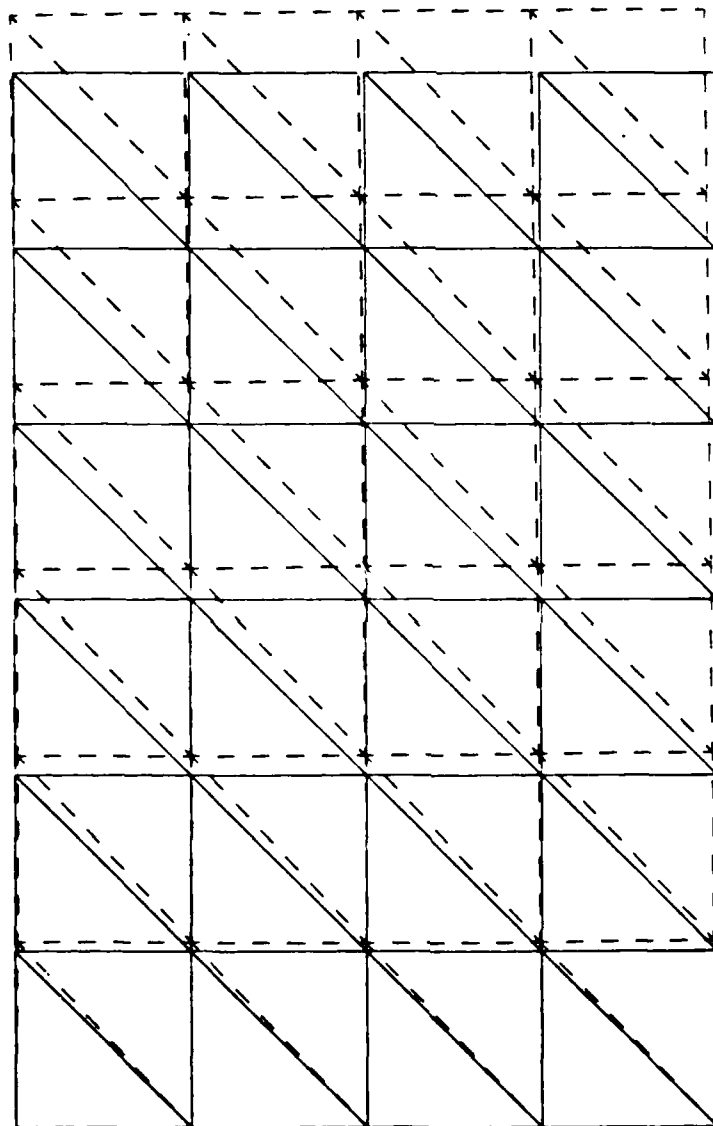
Figure 17. Deformed Shape for Flat Plate Case 1

— Undeformed Shape

--- Deformed Shape

Figure 18. Deformed Shape for Flat Plate Case 2

——— Undeformed Shape
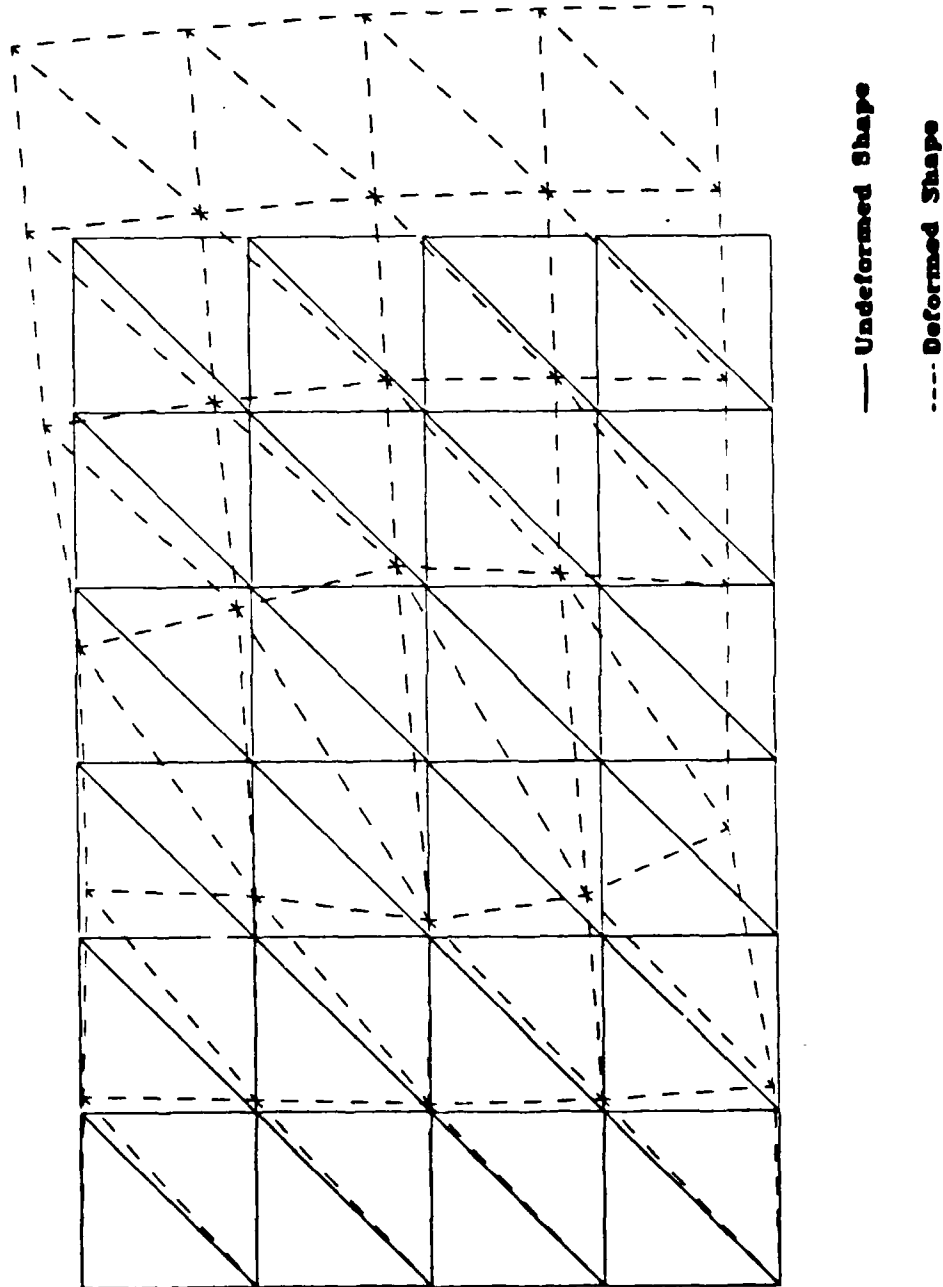
---- Deformed Shape

Figure 19. Deformed Shape for Flat Plate Case 3
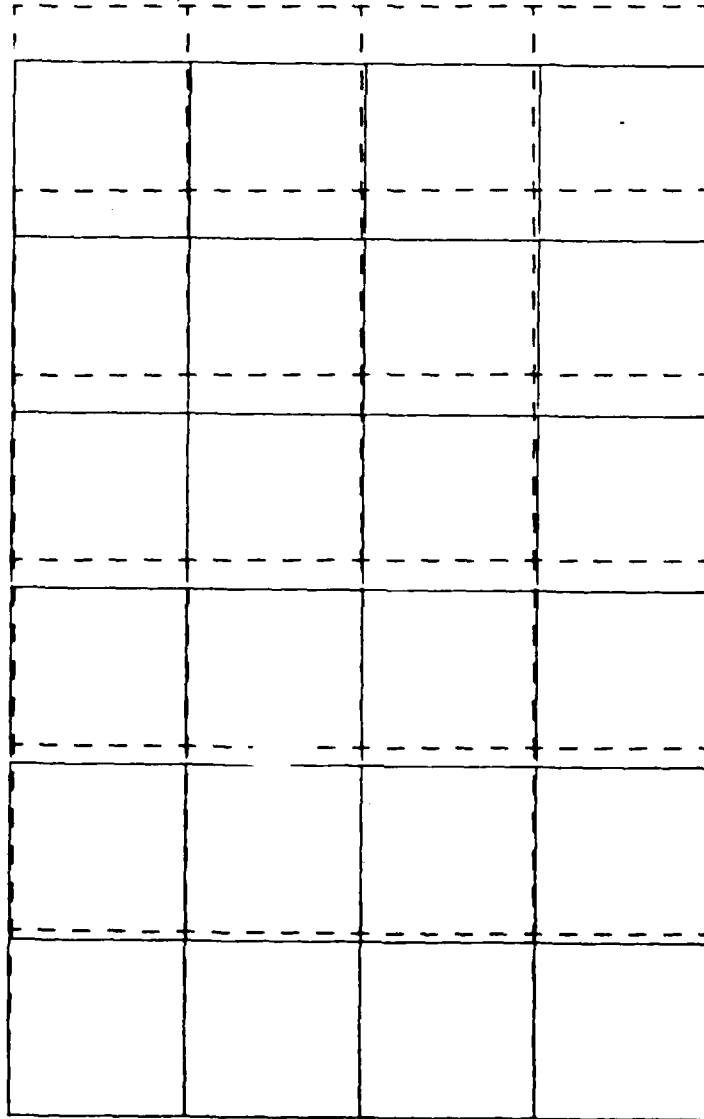
——Underformed Shape

----Deformed Shape

Figure 20. Deformed Shape for Flat Plate Case 4
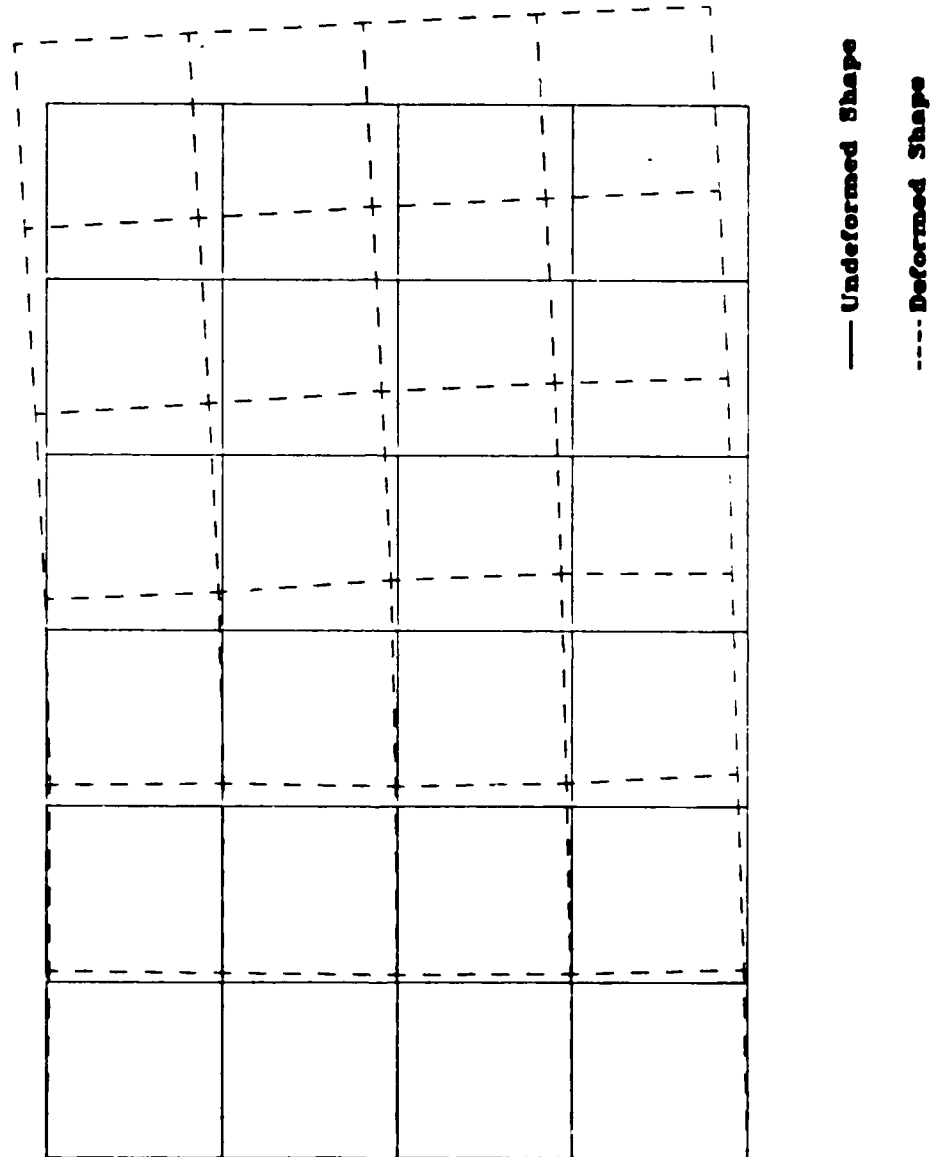
Figure 21. Deformed Shape for Flat Plate Case 5

——— Undeformed Shape

- - - - Deformed Shape

END
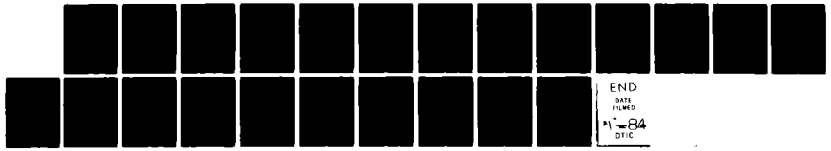
DATE
FILMED

1-84

DTIC
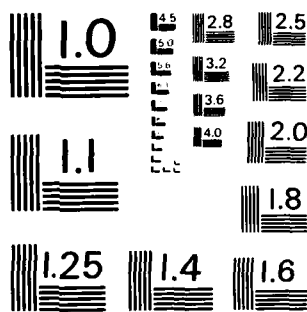
MICROCOPY RESOLUTION TEST CHART
NATIONAL BUREAU OF STANDARDS - 1963 - A
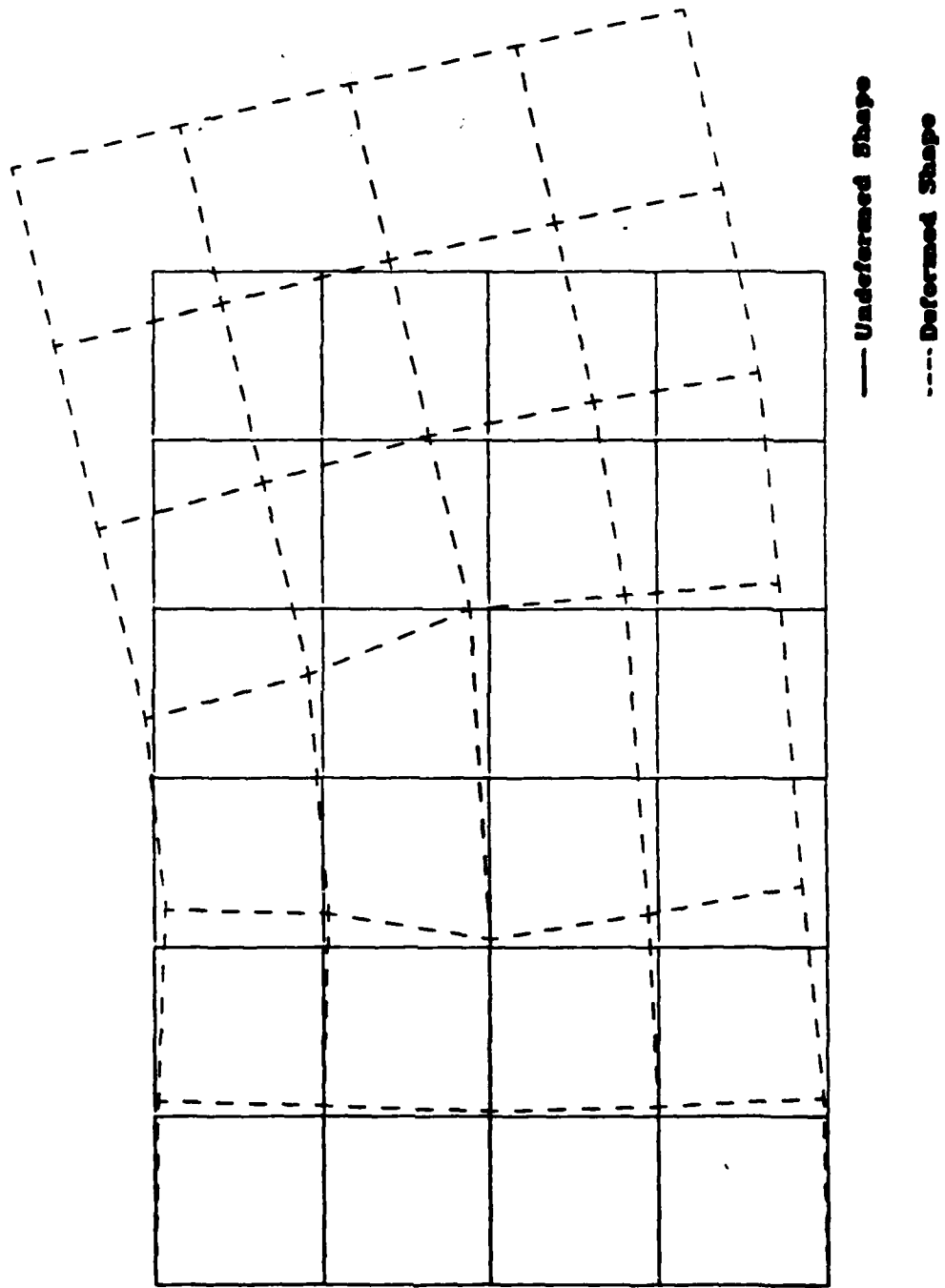
Figure 22. Deformed Shape for Flat Plate Case 6

—— Undeformed Shape

---- Deformed Shape

of damage due to conventional weapons (Ref 5). However, since a temper-
ature change in every element caused the appearance of one or more
damage mechanisms in every element, the iteration extended over all the
elements. Thus the actual change in the stiffness matrix was a major
reduction, requiring an adjustment of every element. As a result, the
stiffness change in each of the reported cases is considered a major
damage condition, and the reanalysis technique proved to be as effective
or better than expected. In a larger structure the damage mechanisms
would be more localized, and the efficiency will become more obvious.
This is shown with the intermediate complexity wing model described
later.

In addition to evaluating the computer run times, the manhours to
set up the models must also be considered. The size of the model also
affects the manhours. Altering the finite element model to reflect a
material loss for the flat plate structure is a simple task requiring
less than 10 minutes clock time. However, to include the Young's modu-
lus changes and the thermal loads is much more time consuming. Since
NASTRAN is a well known finite element code, time comparisons will be
based on the generation of data required for it. Some method must be
used to generate a temperature distribution for each different laser
strike condition. The Young's modulus effects can be incorporated by
specifying that the material is temperature dependent and including an
E versus T table. However, in order for the program to use this data or
to generate the thermal loads, temperatures must either be input for
each node or each element. Without the program developed during this
study, the task of converting the temperature distribution results to
node point temperatures would have to be done by hand. The time

85

required to generate the data in the correct form is about 8 manhours for each strike. Note that even if the laser strike conditions remain the same, a variation of the location of the strike will require this conversion to be made. Therefore, taking a simple model, such as a flat plate with laser strikes in three locations, the program developed in this study shows a manhour savings of three days.

Intermediate Complexity Wing

The second structure was a cantilevered wing shown in Figure 23. This "Intermediate-Complexity Wing" was chosen for study as an illustration of the application of the program in the preliminary design of a lifting surface. It is a typical wing box structure clamped at the root and modeled using rods, triangular membranes, quadrilateral membranes, and shear panels. The top and bottom skins are modeled using triangular and quadrilateral membranes and the spars and ribs by shear panels with rods providing the axial support. The finite element model has 88 nodes and 158 elements (See Figure 24). The applied loading condition was generated by using simplified pressure distributions representative of a subsonic, forward-center-of-pressure loading (Ref 5). The material is assumed to be aluminum with the following properties: $E = 10.5 \times 10^6$ psi, $\nu = 0.3$, $\rho = 0.1$ lbf/in^3.

The damage cases for this structure were constructed as the analysis proceeded by varying the locations and the duration times of the laser strikes using a beam radius of 4.0 in and a peak intensity of $F_0 = 25$ Btu/in^2. The overall objective was to observe the response of the structure as the damage increased to the level where the structure would collapse. The various cases are listed in Table 3. Although each of these four cases results in the loss of skin from the upper surface,

86
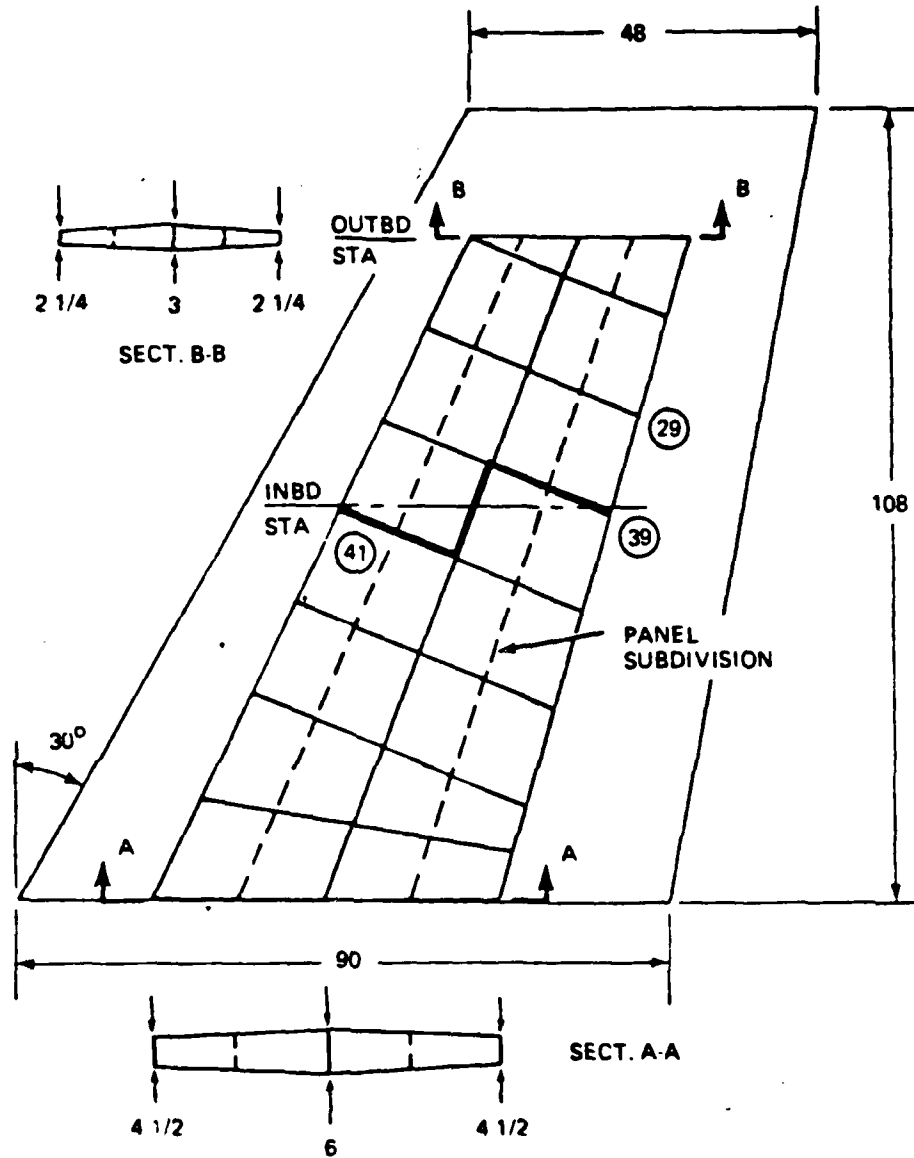
Figure 23. Aerodynamic Planform and Primary Structural
Arrangement of Intermediate-Complexity Wing

87

Notes:

Even numbered nodes are on
bottom surface

Elements:

1-64 top and bottom skins
    (membrane elements)

65-96 shear panels (ribs)

97-119 shear panels (spars)
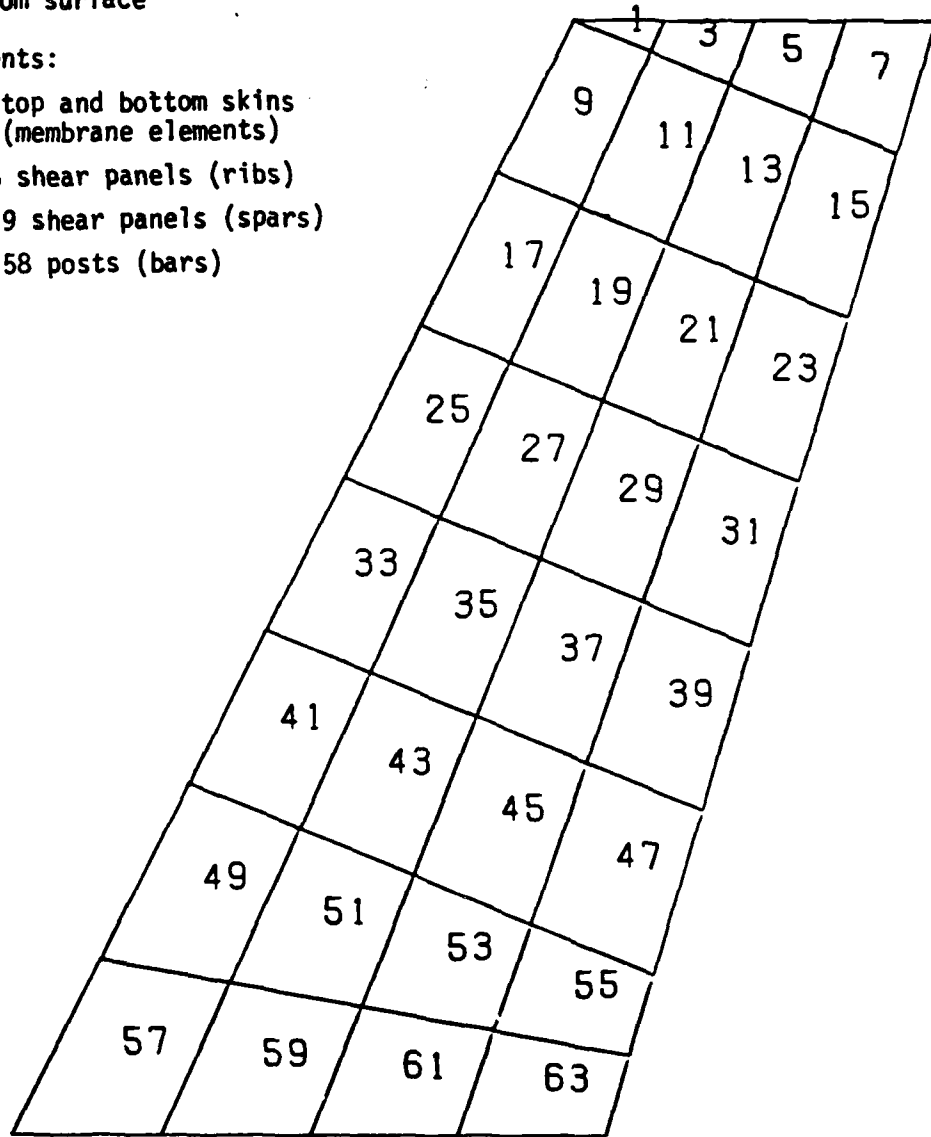
120-158 posts (bars)

Figure 24. Intermediate Complexity Wing Model

Table 3 Description of Intermediate Complexity Wing Cases

Case	Element Struck	% Element Reduced Thru Melt	Strike Endurance (sec)
1	27	100	.455
2	27	100	.455
	29	100	.455
3	25	100	.455
	27	100	.44
	29	100	.40
4	25	100	.40
	27	100	.44
	29	100	.44
	31	63.49	.44

the program can be used to analyze laser strikes on any part of the structure.

Results for the wing cases are shown in Table 4 and the deformed shapes are shown in Figures 25 through 29. This structure is different from the flat plate, because it is three-dimensional and the lower skin, spars, and webs create a pseudo redundancy within the structure. In addition, the overall size of the structure is large enough, 90 in., that the temperature changes are more localized. Therefore a major damage to an element, such as complete removal through melt, and the resulting temperature distribution will generate a localized damage condition and the change in the total structure will be minor. This phenomena can be seen in Case 1 where element 27 has been entirely removed by damage, and yet the maximum displacement for the structure has changed by only 2.3% from the undamaged response.

Case 4 represents a collapse condition. The laser damage induced represents that of a beam moving across the wing at approximately center span. The result is a hole cut through 93.75 percent of the chord at that spanwise location.

Figure 30 reflects the results of all four cases. In this figure the total laser energy added is plotted against the maximum displacement for each case. The plot indicates that an energy threshold exists, above which the damage level increases significantly. The energy added in Cases 1 and 2 are below this threshold while Cases 3 and 4 are above.

An undamaged analysis was performed to give a run time value to use in the operating cost evaluation. The undamaged solution was computed in 3325 10-millisecond tics. For Case 1, with minor damage, the iterative reanalysis program required only 15% of the undamaged solution time

90

Table 4 Intermediate Complexity Wing Results

Case	Reanalysis Max Disp (in)	Reanalysis Strain Energy (Btu/10^6)	Nastran Max Disp (in)	Nastran Strain Energy (Btu/10^6)	Max Disp % Diff	Iter Time (% Undamaged Solution Time)	Cycles	Damage Range
1	14.1157	.1265	14.1585	.1260	.30	15.00	4	Minor
2	15.1215	.1358	15.2251	.1331	.68	42.67	15	Medium
3	19.5280	.1652	19.7947	.1637	1.35	200.	80	Major
4	24.5446	.1997	24.6249	.1943	.32	360.00	150	Major

91
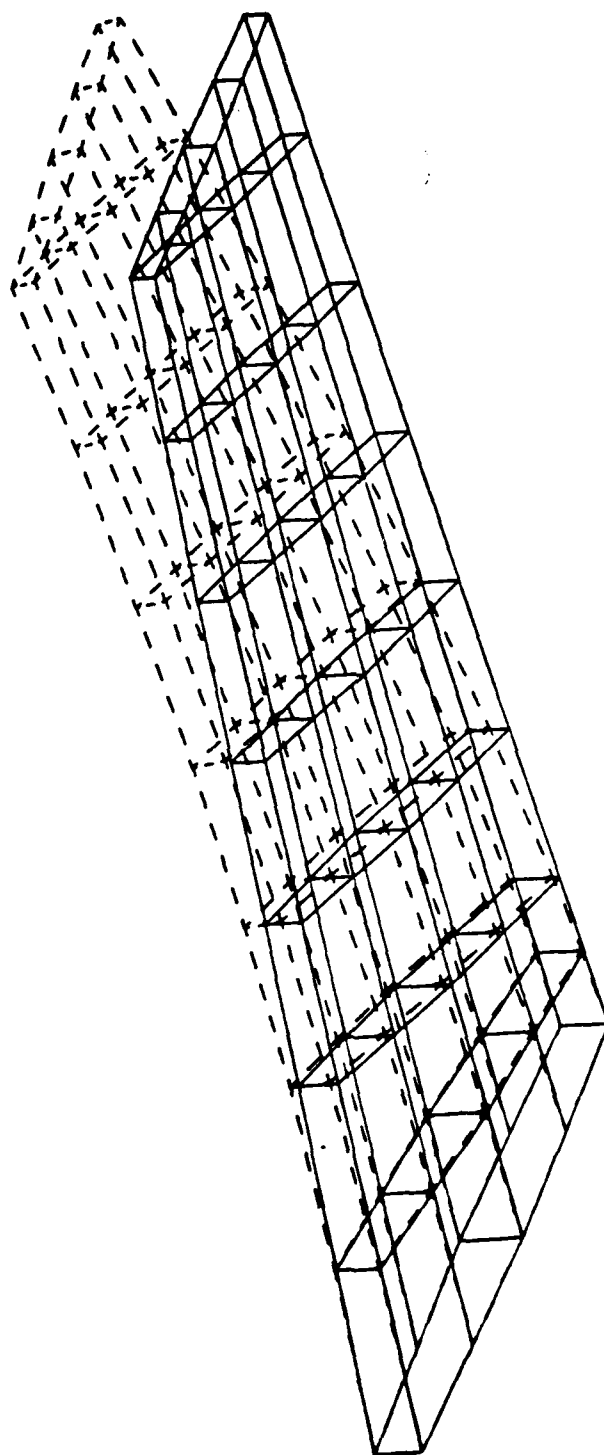
Figure 25. Deformed Shape Undamaged Wing
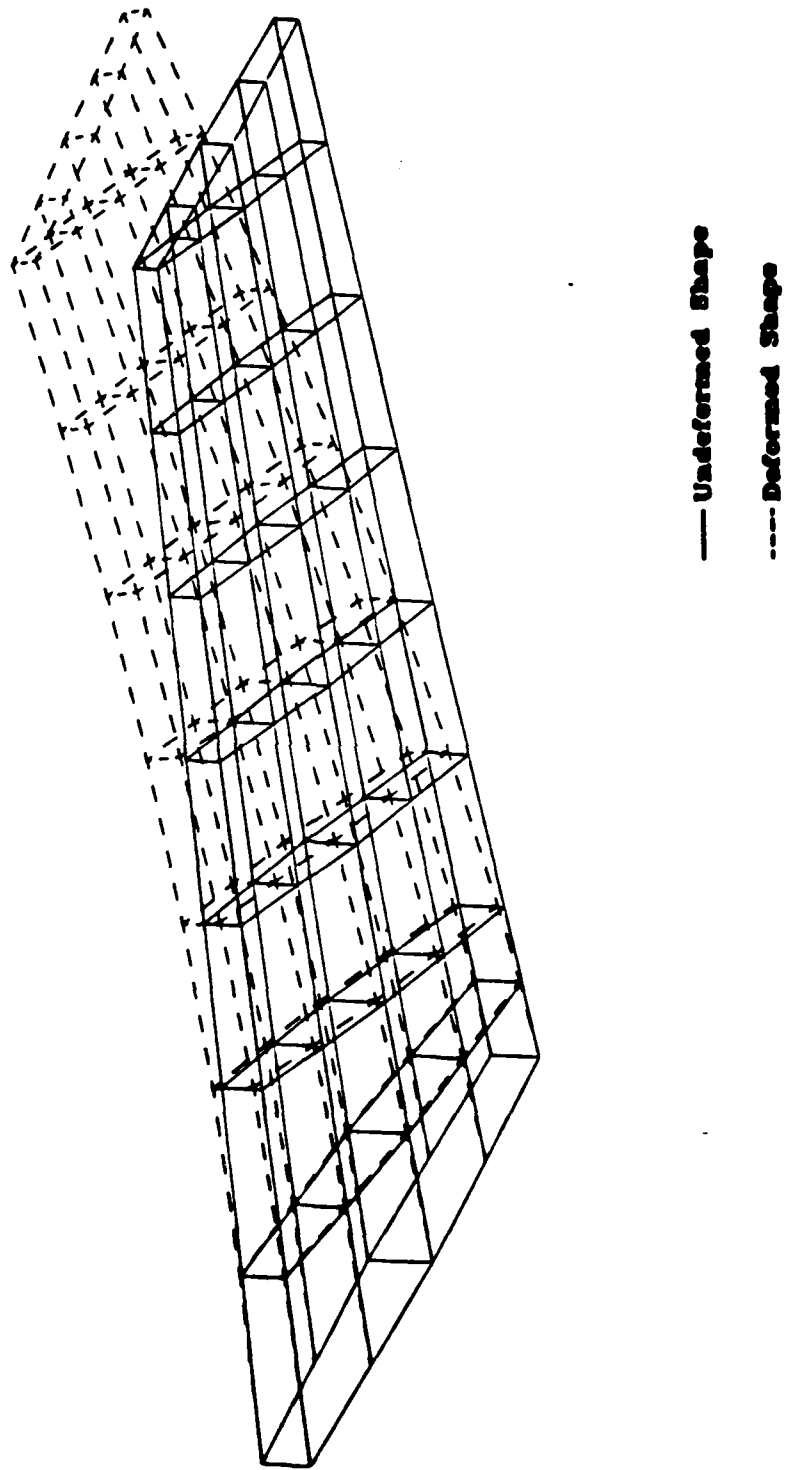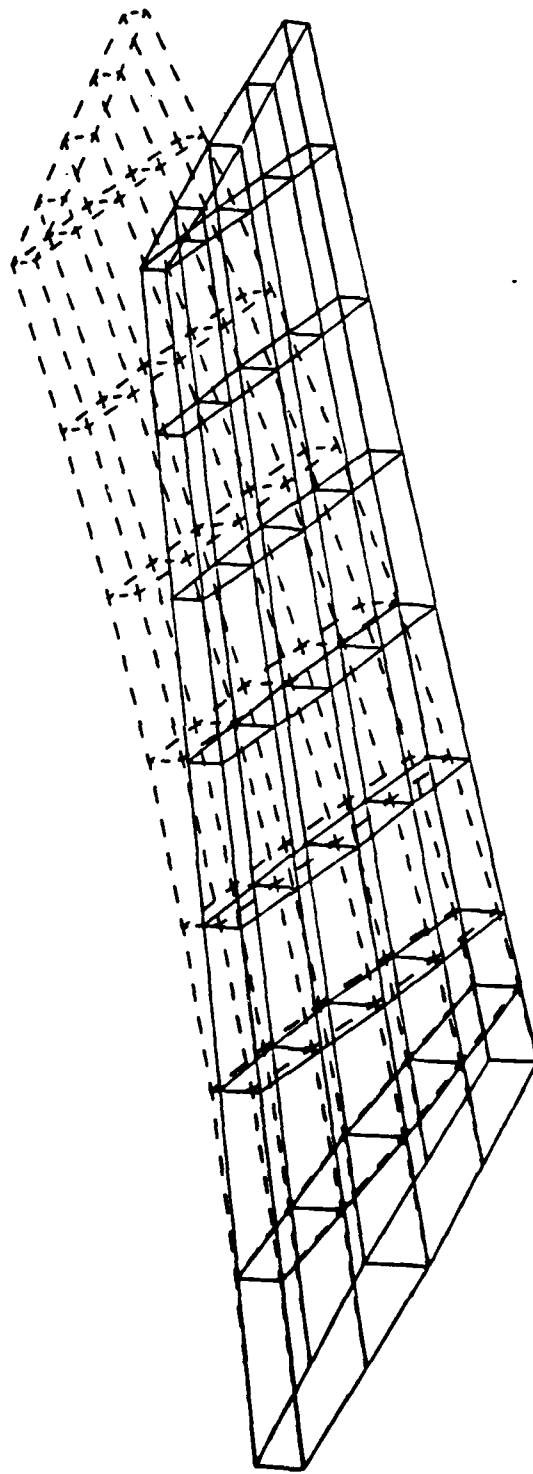
Figure 26. Deformed Shape for Wing Case 1

—Undeformed Shape

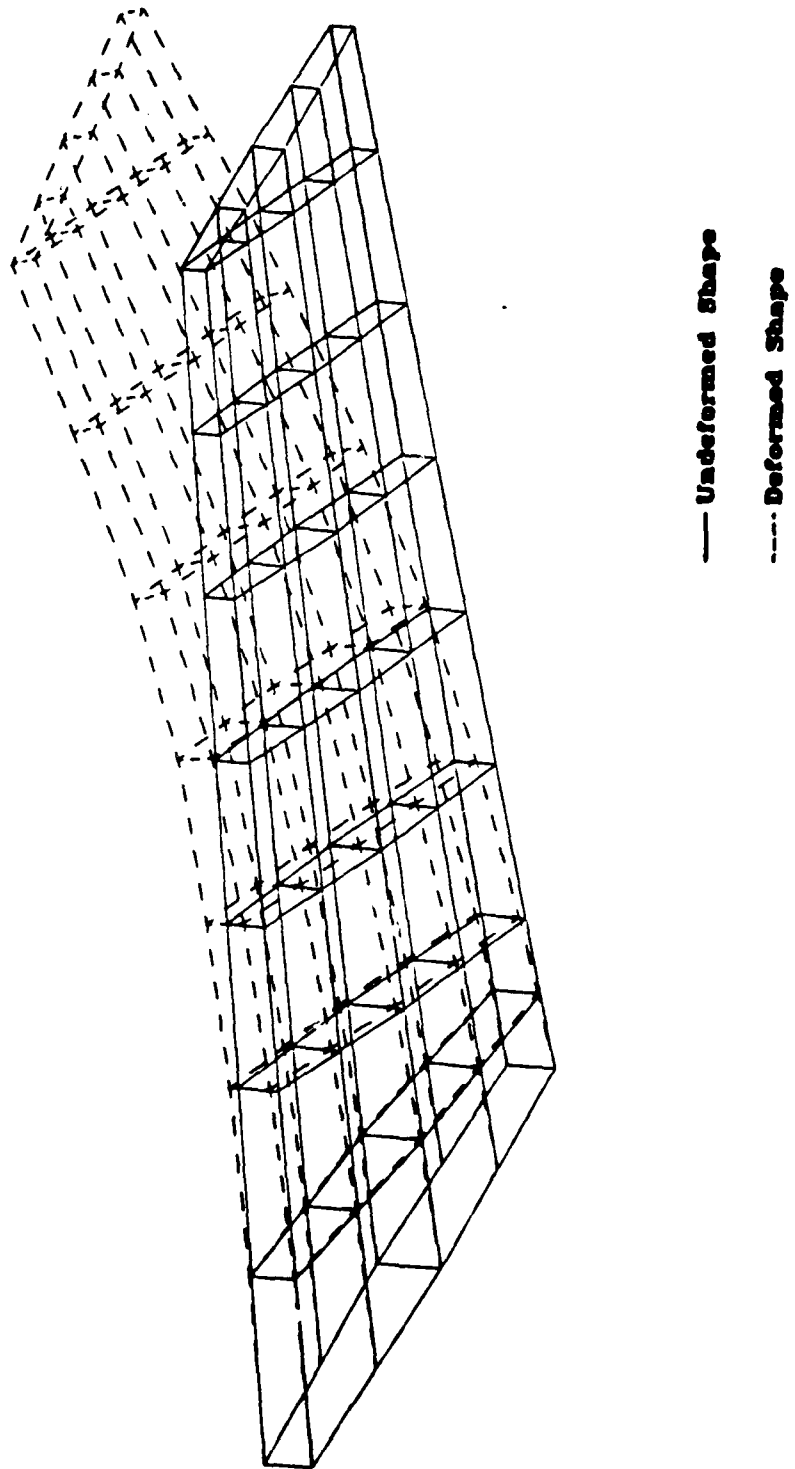---Deformed Shape

Figure 27. Deformed Shape for Wing Case 2

Figure 28. Deformed Shape for Wing Case 3

— Undeformed Shape
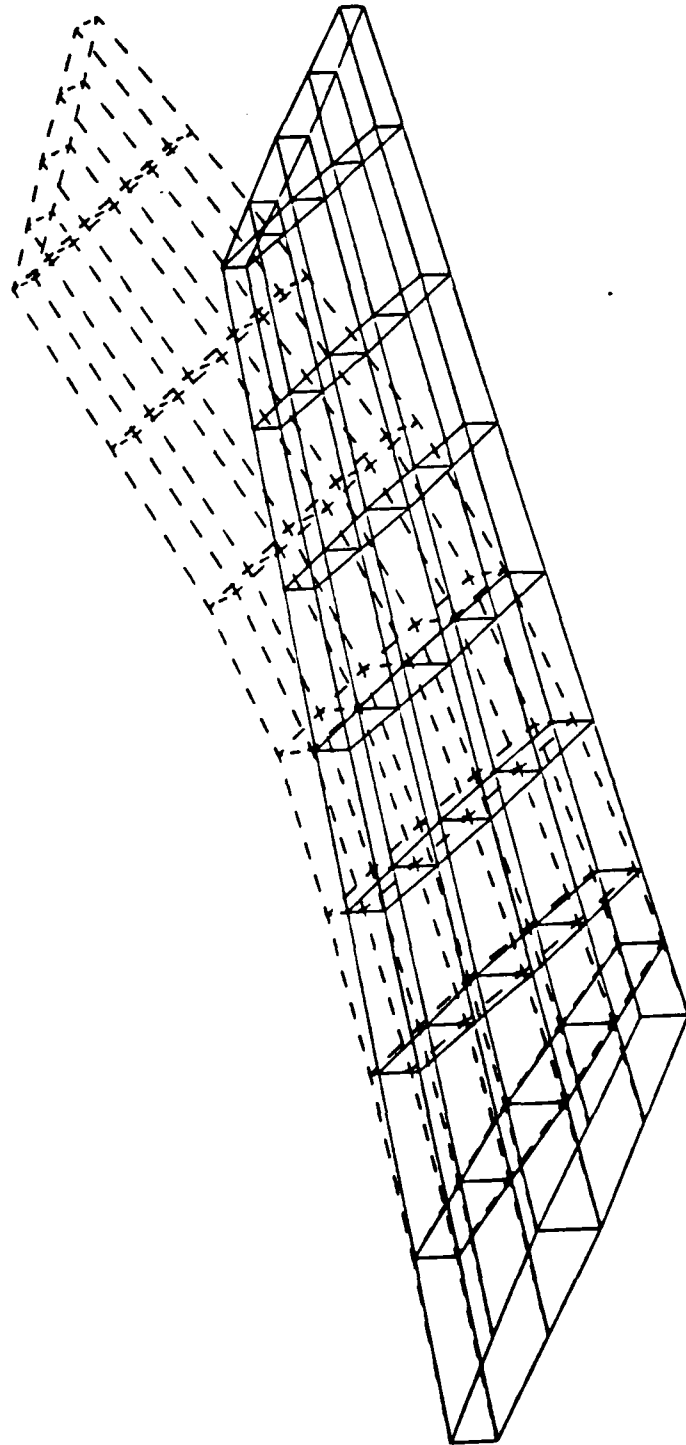
--- Deformed Shape

—— Undeformed Shape

---- Deformed Shape

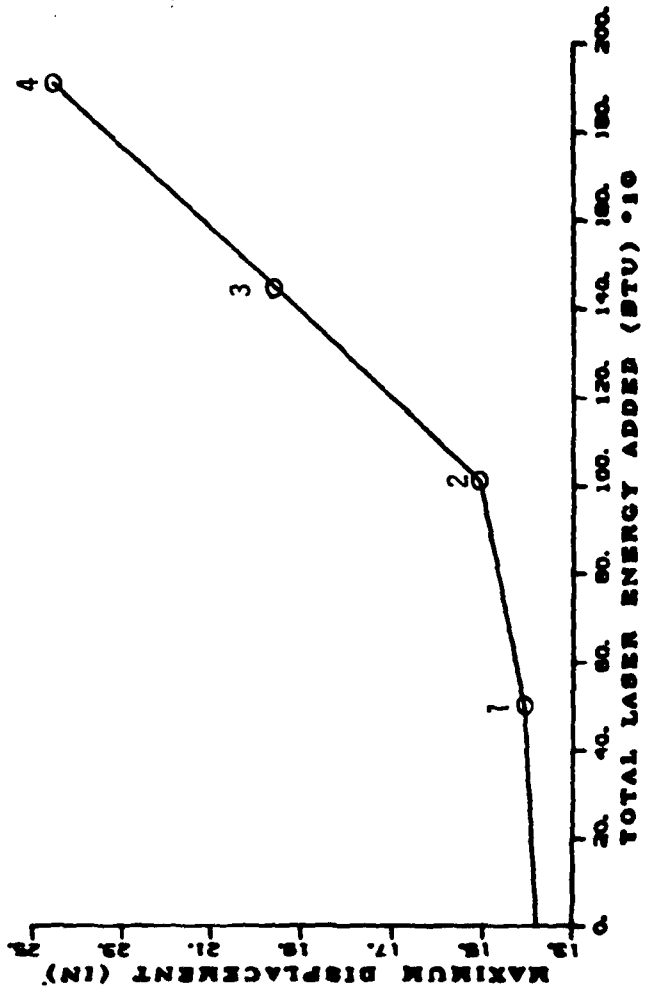Figure 29. Deformed Shape for Wing Case 4

Figure 30. Effect of Laser Energy

to predict the solution. But for Case 4, the collapse condition, the
iteration time was 360%. It must be noted that because the overall size
of the structure is large, the number of elements damaged is small com-
pared to the total number of elements. In such a case the iterative
procedure has shown to be as effective as that reported for damage
incurred through conventional weapons (Ref 5).

When evaluating the manhour savings, once again the size of the
structure is an important consideration. The addition of a third dimen-
sion further complicates the model and increases the time estimation.
As with the flat plate, the change in stiffness of the element due to
melt can be incorporated into NASTRAN data at a relatively low cost
(like 10 minutes). But the temperature calculation, by hand, would take
approximately 3 days. For investigating a large number of damage cases
this program could save a considerable amount of time. For example, the
savings for the four damage cases reported here represent 12 days.

VI Conclusions and Recommendations

Based on the results the reanalysis program with laser damage cal-
culations is capable of predicting the response of a structure under
loads subjected to a laser strike. Due to the numerous assumptions,
the numerical values computed should be treated as tentative, but suited
to the conceptual design phase. From this premise, the following con-
clusions and recommendations are submitted.

Conclusions

1. The reanalysis program developed has met the objective of this
thesis study. That is, it provided a sufficient method for the pre-
diction of structural integrity for a structure encountering a laser
strike.

2.   The findings indicate that for most minor and medium ranges of
damage, the reanalysis technique is an efficient method for analyzing a
large number of damage possibilities.

3. When the manhours are compared for the preparation of multiple
damage models, the reanalysis technique provides substantial savings
over the generation of a model for each case.

Recommendations for Further Development

There are several directions that may be taken at this point. The
intent of this study was to predict the response of an isotropic air-
craft structure. With the current trend to use composites in aircraft
structures, the addition of the capability to analyze these structures
would be a major improvement.

99

The investigation of laser damage is not limited to aircraft structures, but also includes a significant amount of work with missile structures. Including isoparametric elements to allow for the analysis of this type of curved surface is another area of current interest.

Other improvements that are considered to be possible modifications, but would not have a major impact, are including additional structural considerations such as buckling and extending the heat conduction solution to three dimensions.

Bibliography

1. Torvik, Peter J. _A Numerical Procedure for Two Dimensional Heating and Melting Calculations with Applications to Laser Effects_. AFIT TR 72-2. Wright-Patterson Air Force Base, Ohio: Air Force Institute of Technology, March 1972.

2. Torvik, Peter J. _Some Further Numerical Studies of Laser Induced Melting and Vaporization_. AFIT TR 73-1. Wright-Patterson Air Force Base, Ohio: Air Force Institute of Technology, January 1973.

3. Wigglesworth, R. G. _A Numerical Model of Surface Recession Phenomena of Metals Subjected to Laser Radiation in an Aerodynamic Environment_. AFIT Thesis GAW/MC/72-17. Wright-Patterson Air Force Base, Ohio: Air Force Institute of Technology, December 1972.

4. Camburn, G. L. _The Effect of Gravity Upon the "Melt-Through Time" of a Solid Subjected to a High Intensity Laser_. AFIT Thesis GAW/MC/73-6. Wright-Patterson Air Force Base, Ohio: Air Force Institute of Technology, March 1972.

5. Venkayya, V. B., N. S. Khot, and F. E. Eastep. "Vulnerability Analysis of Optimized Structures," _AIAA Journal_, 16(11): 1189-1195 (November 1978).

6. Kirsh, U. and M. F. Rubinstein. "Structural Reanalysis by Iteration," _Computers and Structures_, 2(4): 497-510 (1972).

7. Noor, A. K. and H. E. Lowder. "Approximate Techniques of Structural Reanalysis," _Computers and Structures_, 4(4): 801-812 (1974).

8. Kavlie, D. and G. H. Powell. "Efficient Reanalysis of Modified Structures," _Journal of the Structural Division_, 94(ST1): 377-392 (January 1971).

9. Taylor, R. F. _Automated Design of Damage Resistant Structures, Volume I - Theory and Application_. AFWAL-TR-82-3087. Wright-Patterson Air Force Base, Ohio: Flight Dynamics Laboratory, October 1982.

10. Cook, Robert D. _Concepts and Applications of Finite Element Analysis (Second Edition)_. New York: John Wiley and Sons, Inc., 1974.

11. Gallagher, Richard H. _Finite Element Analysis Fundamentals_. Englewood Cliffs: Prentice-Hall, Inc., 1975.

12. Venkayya, V. B. and Victoria A. Tischler. _"ANALYZE" - Analysis of Aerospace Structures with Membrane Elements_. AFFDL-TR-78-170. Wright-Patterson Air Force Base, Ohio: Air Force Flight Dynamics Laboratory, December 1978.

13. Garvey, S. J. "The Quadrilateral Shear Panel," _Aircraft Engineering_, _XXIII(267)_: 134-144 (May 1951).

14. Fenves, S. J., et al. _Numerical and Computer Methods in Structural Mechanics_. New York: Academic Press, Inc., 1973.

15. MacNeal, R. H. _The NASTRAN Theoretical Manual, Level 16_. NASA SP-221(04). Washington, D.C.: Scientific and Technical Information Division, National Aeronautics and Space Administration, March 1976.

16. Azzi, V. D., Tsai, S. W. "Anisotropic Strength of Composites," _Experimental Mechanics_, September 1965.

17. Torvik, Peter J. _Thermal Response Calculations and Their Role in the Design of Experiments_. AFIT-TR-73-6. WPAFB, Ohio: Air Force Institute of Technology, December 1973.

18. Dusinbeere, G. M. "Numerical Methods for Transient Heat Flow," _Transactions, ASME_, _67_: 707-710 (1945).

19. Ready, John F. _Effects of High-Power Laser Radiation_. New York: Academic Press, Inc., 1971.

20. Carslaw, H. S. and J. C. Jaeger. _Conduction of Heat in Solids_ (Second Edition). Oxford: Oxford University Press, 1959.

VITA

Sheryl Kay Bryan was born April 28, 1951, and raised in the small farming community of Beloit, Kansas. After graduating from Biloit High School in 1969, she entered Kansas State University. In 1974 she enlisted in the United States Air Force and was assigned as a computer programmer to the Air Force Human Resources Laboratory at Lackland Air Force Base. During this assignment she attended the University of Texas on a part-time basis. In 1977 she attended Wichita State University under the Airman's Education and Commissioning Program. In 1979 she received a Bachelor of Science in Aeronautical Engineering, a Bachelor of Science in Computer Science and a commission in the United States Air Force. In 1979 she was assigned to the Air Force Flight Dynamics Laboratory, Wright-Patterson Air Force Base. She is currently a structures development engineer in Analysis and Optimization Branch of the Structures and Dynamics Division.

Permanent address: 701 Banner Circle Drive
                     Salina, Kansas 67401

REPORT DOCUMENTATION PAGE		READ INSTRUCTIONS BEFORE COMPLETING FORM
1. REPORT NUMBER AFIT/GAE/AA/83M-1	2. GOVT ACCESSION NO. A135874	3. RECIPIENT'S CATALOG NUMBER
4. TITLE (and Subtitle) REANALYSIS METHODS FOR STRUCTURES WITH LASER INDUCED DAMAGE		5. TYPE OF REPORT & PERIOD COVERED MS Thesis
		6. PERFORMING ORG. REPORT NUMBER
7. AUTHOR(s) Sheryl K. Bryan		8. CONTRACT OR GRANT NUMBER(s)
9. PERFORMING ORGANIZATION NAME AND ADDRESS Air Force Institue of Technology (AFIT/EN) Wright-Patterson AFB, Ohio 45433		10. PROGRAM ELEMENT, PROJECT, TASK AREA & WORK UNIT NUMBERS Project 2401 Task 240102 Work Unit 24010244
11. CONTROLLING OFFICE NAME AND ADDRESS		12. REPORT DATE March 1983
		13. NUMBER OF PAGES
14. MONITORING AGENCY NAME & ADDRESS(if different from Controlling Office)		15. SECURITY CLASS. (of this report) Unclassified
		15a. DECLASSIFICATION/DOWNGRADING SCHEDULE

16. DISTRIBUTION STATEMENT (of this Report)

Approved for public release; distribution unlimited.

17. DISTRIBUTION STATEMENT (of the abstract entered in Block 20, if different from Report)

18. SUPPLEMENTARY NOTES

Approved for public release; IAW AFR 190.17.

LYNN E. WOLAVER,
Dean for Research and Professional Development
Air Force Institute of Technology (ATC)
Wright-Patterson AFB OH 45433

9 SEP 1983

19. KEY WORDS (Continue on reverse side if necessary and identify by block number)

Finite Element Analysis
Reanalysis Methods
Laser Damage

20. ABSTRACT (Continue on reverse side if necessary and identify by block number)

A reanalysis method to analyze the strength of a structure which has encountered a laser strike is developed. The method accounts for the following types of laser induced damage; 1) loss of structure due to melting; 2) change of material properties due to temperature changes; 3) addition of load due to thermal stress. The program uses heat balance calculations over successive finite time increments on an array of finite elements bisecting the laser beam spot to determine the temperature distribution. These results are then converted to structural stiffness parameters and a finite element based reanalysis method performs

DD FORM 1473 EDITION OF 1 NOV 65 IS OBSOLETE

the structural analysis. The program was found to give accurate results consistent with conducting a separate analysis for each damage condition but with less expenditure of computer time and manhours.